Chemical Geology 421 (2016) 127–142

Contents lists available at ScienceDirect

Chemical Geology

journal homepage: www.elsevier.com/locate/chemgeo

Experimental calibration of silicon and oxygen isotope fractionations between quartz and water at 250 °C by in situ microanalysis of experimental products and application to zoned low $\delta^{30}Si$ quartz overgrowths

Anthony D. Pollington [a,*], Reinhard Kozdon [a,1], Lawrence M. Anovitz [b], R. Bastian Georg [c], Michael J. Spicuzza [a], John W. Valley [a]

[a] WiscSIMS, Department of Geoscience, University of Wisconsin-Madison, 1215 West Dayton Street, Madison, WI 53706, USA
[b] Geochemistry and Interfacial Sciences Group, Oak Ridge National Laboratory, Oak Ridge, TN 37831, USA
[c] Water Quality Centre, Trent University, Peterborough, ON K9J 7B8, Canada

ARTICLE INFO

Article history:
Received 21 June 2015
Received in revised form 9 November 2015
Accepted 11 November 2015
Available online 1 December 2015

Keywords:
Isotope fractionation
$\delta^{30}Si$
$\delta^{18}O$
SIMS
Experimental calibration
Precambrian weathering

ABSTRACT

The interpretation of silicon isotope data for quartz is hampered by the lack of experimentally determined fractionation factors between quartz and fluid. Further, there is a large spread in published oxygen isotope fractionation factors at low temperatures, primarily due to extrapolation from experimental calibrations at high temperature. We present the first measurements of silicon isotope ratios from experimentally precipitated quartz and estimate the equilibrium fractionation vs. dissolved silica using a novel in situ analysis technique applying secondary ion mass spectrometry to directly analyze experimental products. These experiments also yield a new value for oxygen isotope fractionation. Quartz overgrowths up to 235 μm thick were precipitated in silica–H_2O–NaOH–NaCl fluids, at pH 12–13 and 250 °C. At this temperature, $1000\ln\alpha^{30}Si(Qtz\text{–}fluid) = 0.55 \pm 0.10‰$ and $1000\ln\alpha^{18}O(Qtz\text{–}fluid) = 10.62 \pm 0.13‰$, yielding the relations $1000\ln\alpha^{30}Si(Qtz\text{–}fluid) = (0.15 \pm 0.03) * 10^6/T^2$ and $1000\ln\alpha^{18}O(Qtz\text{–}fluid) = (2.91 \pm 0.04) * 10^6/T^2$ when extended to zero fractionation at infinite temperature. Values of $\delta^{30}Si(Qtz)$ from diagenetic cement in sandstones from the basal Cambrian Mt. Simon Formation in central North America range from 0 to −5.4‰. Paired $\delta^{18}O$ and $\delta^{30}Si$ values from individual overgrowths preserve a record of Precambrian weathering and fluid transport. The application of the experimental quartz growth results to observations from natural sandstone samples suggests that precipitation of quartz at low temperatures in nature is dominated by kinetic, rather than equilibrium, processes.

Abbreviations/Definitions

$\delta^{18}O(Qtz) = [^{18}O/^{16}O(Qtz)]/[^{18}O/^{16}O(VSMOW)\ 1] \times 1000$
$\alpha^{18}O(Qtz\text{-}H_2O) = [^{18}O/^{16}O(Qtz)]/[^{18}O/^{16}O(H_2O)]$
$\varepsilon^{18}O(Qtz\text{-}H_2O) = [\alpha^{18}O(Qtz\text{-}H_2O)\ -\ 1] \times 1000 \approx 1000\ln\alpha^{18}O(Qtz\text{-}H_2O)$
DQ = detrital quartz
OQ = overgrowth quartz
$\Delta^{18}O(earlyOQ\text{-}lateOQ) = \delta^{18}O$(early overgrowth quartz i.e., closest to detrital grain) $- \delta^{18}O$(late overgrowth quartz i.e., farthest from detrital grain)
Silicon isotopes follow equivalent nomenclature to oxygen e.g.,
$\delta^{30}Si(Qtz) = [^{30}Si/^{28}Si(Qtz)]/[^{30}Si/^{28}Si(NBS\text{-}28)\ -\ 1] \times 1000$

1. Introduction

Since Urey (1947) first proposed the use of isotope fractionation as a method for determining paleo-temperatures, there have been hundreds of calibrations published for the light stable isotope fractionation between different phases (Chacko et al., 2001). Fractionation factors can be determined experimentally, empirically, or derived theoretically, and vary with element and the phases involved. Knowledge of the temperature dependence of the fractionation for the system being studied is of great importance. Recent analytical advancements have led to increased

* Corresponding author at: Nuclear and Radiochemistry, Los Alamos National Laboratory, PO Box 1663 MSJ514, Los Alamos, NM 87545, USA.
E-mail address: pollington@lanl.gov (A.D. Pollington).
[1] Present address: Lamont-Doherty Earth Observatory of Columbia University, Palisades, NY 10964, USA.

http://dx.doi.org/10.1016/j.chemgeo.2015.11.011
0009-2541/

precision of analysis and a renewed interest in silicon isotope systematics of quartz and many other minerals. Whereas oxygen isotopes yield information about the thermal and fluid history of the mineral, silicon isotopes can constrain the sources of dissolved ions and fluids. An understanding of the O and Si isotope fractionations associated with the formation of quartz is essential to studies of this common mineral.

There are relatively few published estimates for the fractionation of silicon isotopes between silica and fluids (Douthitt, 1982; Li et al., 1995; De La Rocha et al., 1997; De La Rocha, 2003; Geilert et al., 2014; Roerdink et al., 2015), and there are no experimental determinations of silicon isotope fractionation factors between quartz and aqueous silicon. Most estimates are based on measurements of natural samples (Douthitt, 1982; De La Rocha, 2003). The experimental calibrations that do exist are principally for cultured diatoms (De La Rocha et al., 1997), which may be hydrous, non-crystalline and influenced by vital effects. Calibrations that are experimental and abiogenic (Li et al., 1995; Geilert et al., 2014; Roerdink et al., 2015) precipitated amorphous silica (not quartz) from a solution and may have very different fractionation factors than crystalline quartz.

In contrast to silicon, numerous experimental, empirical and theoretical studies have been performed to determine the oxygen isotope fractionation between quartz and water over a range of temperatures (e.g., Clayton et al., 1972; Shiro and Sakai, 1972; Bottinga and Javoy, 1973; Kawabe, 1978; Matsuhisa et al., 1979; Zheng, 1993; Sharp and Kirschner, 1994; Hu and Clayton, 2003). For experiments at higher temperatures (400–800 °C), calibrations were fit to the experimental results. In experiments performed at lower temperatures (200–400 °C), calculations of the percentage of isotope exchange show that isotopic equilibrium was not achieved (Clayton et al., 1972; Matsuhisa et al., 1979; Hu and Clayton, 2003). At high temperatures, individual calibrations are in relatively good agreement (<1‰ variability above 400 °C). However, extrapolation of calibrations to lower temperature leads to differences in the calculated fractionation factors that vary by over 16‰ below 50 °C (Fig. 1).

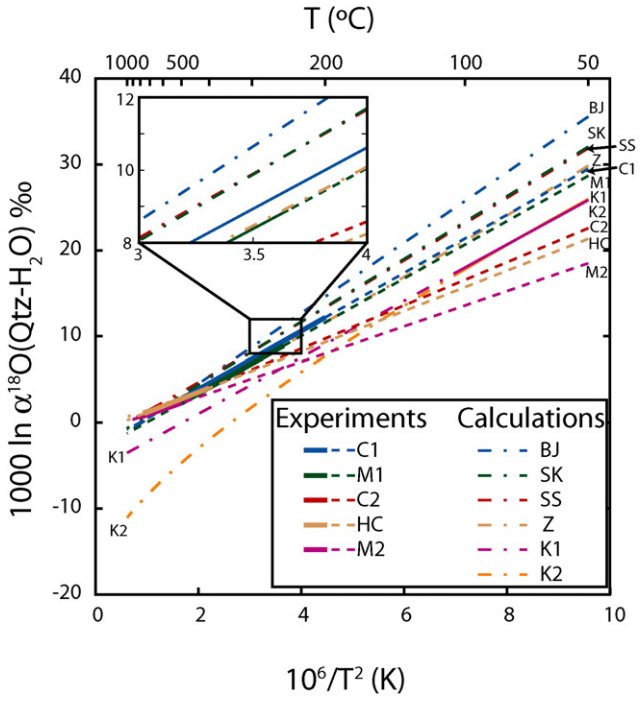

Fig. 1. Comparison of calibrations of quartz–water oxygen isotope fractionation. Bold line segments for previous studies represent the temperature range over which experiments were conducted. Dashed lines are extrapolations of experimental calibrations. Dash-dot lines are based on theoretical calculations or recalculations of previously published experiments. Curves are plotted using fractionation factors published in each study and are extrapolated to 50 °C. At high temperatures, calibrations based on experiments are in relatively good agreement (<1‰ above 400 °C), however at low temperatures, there is extreme disagreement between the extrapolated lines (max. 16‰ at 50 °C). Inset highlights the discrepancy between calibrations at the temperature range of experiments in this study (250 °C; Supplemental Fig. S3). The abbreviations for each calibration are: C1 = 200–500 °C, Clayton et al. (1972); M1 = 250–500 °C, Matsuhisa et al. (1979); C2 = 500–750 °C, Clayton et al. (1972); HC = 400–750 °C, Hu and Clayton (2003); M2 = 500–800 °C, Matsuhisa et al. (1979); BJ = Bottinga and Javoy (1973); SK = Sharp and Kirschner (1994); SS = Shiro and Sakai (1972); Z = Zheng (1993); K1 = 2-term fit, Kawabe (1978); K2 = 3-term fit, Kawabe (1978). Calibrations from Clayton et al. (1972) use recalculated values from Friedman and O'Neil (1977).

Partial exchange at lower-temperatures potentially introduces uncertainty into the calculated fractionation factors. Previous studies have been conducted as exchange reactions of fine-grained powder, with the final product being measured as a bulk sample. If quartz powder does not fully equilibrate at the maximum temperature of an experiment, then the core of each grain may have an inherited value, potentially leading to large errors in the value of experimentally reacted quartz. The percent of reaction has been calculated and then extrapolated to the fractionation for 100% reaction by making use of measurements of three isotopes of oxygen (Matsuhisa et al., 1978) and the kinetics of partial-exchange reactions (Clayton et al., 1989). However, if overgrowths of micrometer-scale can be grown, then in situ analysis of experimental products makes it possible to measure only quartz precipitated during the experiment and completely avoid unreacted material.

In addition to uncertainties introduced by extrapolation over large temperature ranges, the "salt effect" of dissolved species must be considered. The fractionation between a mineral and pure water is generally different from the fractionation between a mineral and aqueous solution (e.g., Horita et al., 1993a, 1993b, 1995; Hu and Clayton, 2003). Different dissolved species and concentrations may account for some of the discrepancies between previous calibrations, both for oxygen and silicon isotopes. While the salt effect on oxygen isotope fractionation between quartz and water is often relatively small (usually <1‰; Hu and Clayton, 2003) and cannot account for the full 16‰ variability between calibrations at 50 °C, small uncertainties from high temperature calibrations are magnified when extrapolating outside the range of temperatures of the experiments.

In this paper, new experimental growth of quartz in a solution of pH ~ 12 in 126 days at 250 °C on a seed crystal and for the fluid from which that quartz precipitated is reported. We show that in situ stable isotope measurement of experimentally precipitated material is a useful tool for the low-temperature calibration of fractionation factors. Direct fluorination and oxygen isotope analysis of 5 μl aliquots of fluid from experiments are described, which avoids analytical uncertainties associated with dissolved salts. Finally, the new fractionation factors are applied to high spatial-resolution, high precision, paired silicon and oxygen isotope data for the Cambrian Mt. Simon Sandstone. Combined $\delta^{30}Si$ and $\delta^{18}O$ from diagenetic cements constrain the chemical weathering and thermal history of a rock, and with the results of the new experiments the question of equilibrium vs. kinetic processes during weathering and precipitation is tested.

2. Methods and sample description

2.1. Quartz growth experimental setup

To determine the fractionation factors for quartz precipitated from an aqueous solution, a set of experiments was designed to crystallize quartz under controlled thermal and chemical conditions. The reactions that control quartz and amorphous silica precipitation/dissolution are:

$$SiO_2(\text{amorph.silica}) + 2H_2O \Leftrightarrow H_4SiO_4^\circ \quad (1)$$

$$SiO_2(\text{quartz}) + 2H_2O \Leftrightarrow H_4SiO_4^\circ \quad (2)$$

$$SiO_2(\text{amorph.silica}) + OH^- + H_2O \Leftrightarrow H_3SiO_4^- \quad (3)$$

$$SiO_2(\text{quartz}) + OH^- + H_2O \Leftrightarrow H_3SiO_4^- \quad (4)$$

$$SiO_2(\text{amorph.silica}) + OH^- + \tfrac{1}{2}H_2O \Leftrightarrow H_2SiO_4^{2-} \quad (5)$$

$$SiO_2(\text{quartz}) + OH^- + \tfrac{1}{2}H_2O \Leftrightarrow H_2SiO_4^{2-}. \quad (6)$$

The equilibrium constants for these reactions vary depending on the solid phase, pH, temperature, and the concentration of dissolved material (e.g., salts). At pH values below ~9, $H_4SiO_4^\circ$ dominates the concentration of dissolved Si ([Si]) (Stumm and Morgan, 1996; Wesolowski et al., 2004). At pH values between ~9 and 11, there is less $H_4SiO_4^\circ$ than $H_3SiO_4^-$ and at even higher pH, the dominant species may be $H_2SiO_4^{2-}$ (e.g., Fig. 7.5 of Stumm and Morgan, 1996). The present experiments were controlled at pH = 12–13 by the addition of NaOH, the dissolution of amorphous silica and precipitation of quartz (Fig. 2B).

Three aqueous solutions were used in this study (Tables 1A, 1B, 1C): (Soln. A) 0.1 m NaOH & 0.1 m NaCl with excess ground silica glass (SG-1); (Soln. B) 0.1 m NaOH with excess SG-1; and (Soln. C) concentrated sodium silicate solution (0.17 wt.% Si). There is little temperature dependence for the solubility of silica in 0.1 m NaOH solutions (A and B) below 300 °C (Fig. 2A). Thus, a silica-saturated solution can be prepared at room temperature and heated to various working temperatures without significantly affecting the degree of saturation. This minimizes problems of precipitation during quenching. For solution B, 50 ml of 0.1 m NaOH was heated in a Teflon beaker on a hotplate at ~80 °C with 597 mg ground silica glass (<10 μm diameter) for 3 days to produce a solution saturated relative to amorphous silica. To prepare solution A, 16 ml of solution B was transferred to a separate Teflon beaker and 513 mg NaCl was added for a nominal concentration of 0.5 m NaCl. Solution C was prepared by diluting 1.4 g stock sodium silicate solution (Fisher number SS338-1, nominal concentration 9.1 wt.% Na_2O, 29.2 wt.% SiO_2, equivalent to 13.6 wt.% Si) with 98 g N_2-sparged purified, deionized (Milli-Q) water. All solutions were saturated with respect to amorphous silica at a concentration of 1700–1800 ppm (mg/kg) Si (Tables 1A, 1B, 1C) and oversaturated with respect to quartz (Fig. 2B).

At room temperature, the solutions were divided into individual reaction vessels, as well as aliquots for isotope measurements of reactants. Reaction vessels had a flat-bottomed open-topped Teflon liner inside a stainless steel vessel modified from a VCR vacuum fitting (Anovitz et al., 2004). The dimensions of the metal vessel were 22 mm interior diameter, 47 mm tall (Supplemental Fig. S1). The Teflon liner fit into the metal vessel and the volume of the Teflon liner was ~14 ml.

Each individual run contained 4 ml of fluid, as well as a piece of seed quartz, which acted as a substrate for the growth of new quartz. The quartz seeds used in all the experiments were wafers (5 mm thick, 2–5 mm wide) cut perpendicular to the C-axis of a single crystal (Fig. 3) because growth in the C-direction is much faster than growth in other orientations (Lander et al., 2008). The parallel faces of each wafer were polished with a series of diamond polishing pads (6, 3, then 1 μm), followed by 0.05 μm colloidal alumina to remove polishing damage that might affect nucleation and growth of new quartz. Solutions A and B also contained ~100 mg of excess ground silica glass in each reaction vessel. The ground glass excess ensured that as silicon was removed from solution to precipitate quartz, amorphous silica would dissolve maintaining the concentration and $\delta^{30}Si$ of the fluid. The amount of Si and O in the liquid used in each experiment was large in proportion to the amount of precipitated solid material (the ratio of moles of Si and O in liquid + excess powder to Si and O in precipitated quartz is ~400,000 for both elements).

Nine vessels were prepared, three with each of the three starting solutions, so that the reaction progress could be monitored at three intervals over the course of the experiments. All reactants were added to the reaction vessels, sealed, weighed, and placed overnight in a vacuum oven at 60 °C. The vessels were then cooled to room temperature and weighed again to confirm that no leaks had occurred. The vessels were then placed in a preheated furnace at 250 °C with a digitally controlled temperature range of ~±0.5 °C. In addition to the nine experiments at

Table 1A
Summary of quartz experiments at 250 °C and starting materials.

	Starting solution	Days in furnace	Final solids after experiment	[Si] (mg/kg)[b]
Starting materials				
SG-1[a]				
Soln. A	Ground glass, NaOH, NaCl			1768
Soln. B	Ground glass, NaOH			
Soln. C	Concentrated sodium silicate solution			1709
Experiments				
250-1	A	20	Powder; seed crystal.	
250-2	A	86	100 μm Qtz overgrowth; powder; seed crystal.	1789
250-3	A	126	235 μm Qtz overgrowth; powder; seed crystal.	1847
250-4	B	86	Powder; seed crystal.	
250-5	B	126	Powder; seed crystal.	
250-6	B	126	Analcime; powder; seed crystal.	
250-7	C	22	1 μm Qtz overgrowth; seed crystal.	
250-8	C	85	5 μm Qtz overgrowth; seed crystal.	
250-9	C	126	8 μm Qtz overgrowth; doubly terminated Qtz (1–50 μm); Analcime; seed crystal.	770

[a] SG-1 is ground silica glass for solutions A and B.
[b] Silicon concentration in solution. Values for experiments were measured after the experiments.

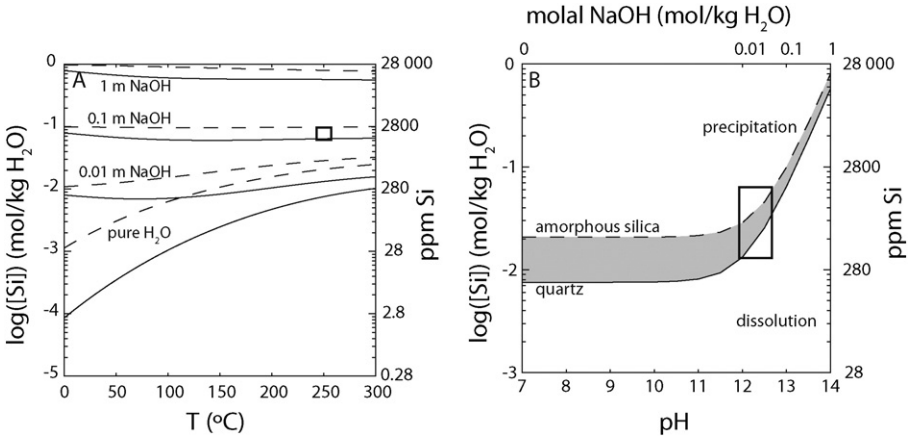

Fig. 2. (A) Concentration at saturation for dissolved silica calculated as a function of temperature for varying concentrations of NaOH in aqueous solution (Wesolowski et al., 2004; Eqs. (1)–(6)). Solid lines are solubility of quartz, dashed lines are for amorphous silica. Note that solubility is relatively constant below 300 °C for 0.1 m NaOH; experimental solutions in this study are all ~0.1 m NaOH. (B) Concentration of dissolved silica as a function of pH or NaOH concentration for 250 °C. The gray shaded conditions between the quartz and amorphous silica curves will result in dissolution of amorphous silica and precipitation of quartz. Boxes in each panel represent the conditions of these experiments.

Table 1B
Summary of oxygen isotope data for quartz experiments at 250 °C. All quartz analyses are SIMS except $\delta^{18}O$(Qtz) of powder.

	$\delta^{18}O$(Qtz) powder ‰VSMOW[b]	$\delta^{18}O$(Qtz) ‰VSMOW average SIMS	$\delta^{18}O$(Qtz) 2SE ‰ SIMS	$\delta^{18}O(H_2O)$ average ‰VSMOW	$\delta^{18}O(H_2O)$ 2SD ‰[c]	$\varepsilon^{18}O$ (Qtz–H_2O) ‰	2SD (Qtz–H_2O) ‰
Starting materials							
SG-1[a]	9.94						
Soln. A				−7.02 (n = 2)	0.20		
Soln. B							
Soln. C				−8.77 (n = 2)	0.17		
Experiments							
250-1							
250-2	7.34	4.27 (n = 18)	0.06	−6.37 (n = 2)	0.12	10.64	0.13
250-3	4.30	4.07 (n = 87)	0.06	−6.52 (n = 3)	0.22	10.59	0.23
250-4	5.11						
250-5	5.20						
250-6	29.68						
250-7							
250-8							
250-9				−8.48 (n = 2)	0.17		

Numbers in parentheses are the number of analyses (individual SIMS spots or replicate H_2O analyses) used to calculate average values.
[a] SG-1 is the ground silica glass added to solutions A and B.
[b] Precision on $\delta^{18}O$ powder analyses by laser fluorination is ±0.21‰ 2SD based on 8 measurements of UWG-2 standard run at the same time as experimental powders.
[c] 2SD on $\delta^{18}O(H_2O)$ is the higher of the analytical precision (0.12‰) or the 2SD based on replicate analyses of the given solution.

250 °C, we also conducted nine experiments at 175 °C and seven experiments at 100 °C using the same three solutions. Upon inspection after 419 days for 100 °C and 219 days for 175 °C, no apparent quartz had precipitated on the seed crystal; these experiments are not considered further in this study.

The 250 °C reaction vessels were heated for times of 20, 86, and 126 days (Tables 1A, 1B, 1C). At the end of each run, the vessel was removed from the furnace and cooled to room temperature in a water bath. The majority of quenching occurred in the first minute, but vessels were allowed to cool for 45 min to ensure full cooling across the vessel. When the vessel was at room temperature, it was dried and again weighed to confirm no loss of fluid due to leakage. The vessels were opened and the fluids were immediately sealed in multiple glass capillary tubes of 3–5 μl each for $\delta^{18}O$ analysis. Aliquots for $\delta^{30}Si$ analysis were extracted and stored in polyethylene bottles. Because the [Si] of the solutions was much higher than that needed for multi-collector inductively coupled plasma mass spectrometer (MC-ICP-MS) analysis, solutions were diluted to a nominal concentration of 10 ppm (mg/kg) Si with 71 μl of experimental solution and 20 ml of N_2-sparged Milli-Q water. This dilution also prevented later precipitation of silicon-bearing species between the end of the experiment and the time of analysis. The remainder of each solution was sealed in glass ampules. The products from experiments using solutions A and B had excess powder, which was also collected and dried in an oven at ~60 °C overnight. The wafers of seed quartz were removed, rinsed with distilled water and isopropyl alcohol and dried at ~60 °C overnight.

2.2. Sample characterization

2.2.1. Experimental product characterization

Each wafer of seed quartz was examined using a Hitachi 3400 scanning electron microscope (SEM) at the University of Wisconsin. Immediately after opening the reaction vessels, the dried wafers were examined in environmental mode (~50 Pa) with no conductive coating to describe the morphology of any new growth and to determine the best location to cut the wafer for observation in cross-section. All surfaces were imaged by secondary electrons (SE) using an environmental secondary electron detector (ESED) and backscattered electrons (BSE), characterized with respect to morphology, and chemical composition was determined by energy dispersive X-ray spectroscopy (EDS). The wafer was then cast in epoxy, cut and polished parallel to the C-axis of the seed-quartz crystal and re-examined by SEM to observe new quartz growth in cross-section. The polished, uncoated cross-sections were analyzed in environmental mode by electron backscatter diffraction (EBSD) to confirm the mineral identity of the seed and precipitated

Table 1C
Summary of silicon isotope data for quartz experiments at 250 °C measured by SIMS for quartz and ICP-MS for solutions.

	$\delta^{30}Si$(Qtz) average SIMS ‰NBS28	$\delta^{30}Si$(Qtz) 2SE SIMS ‰	$\delta^{30}Si$(fluid) ICP-MS ‰NBS28	$\delta^{30}Si$(fluid) 2SD ‰ ICP-MS	$\varepsilon^{30}Si$ (Qtz–fluid) ‰	2SD (Qtz–fluid) ‰
Starting materials						
SG-1[a]						
Soln. A			0.06	0.10		
Soln. B						
Soln. C			0.27	0.10		
Experiments						
250-1						
250-2	0.21 (n = 16)	0.14	−0.30	0.10	0.51	0.17
250-3	0.43 (n = 68)	0.06	−0.15	0.10	0.58	0.12
250-4						
250-5						
250-6						
250-7						
250-8						
250-9			0.22	0.11		

Numbers in parentheses are the number of analyses (individual SIMS spots) used to calculate average values.
[a] SG-1 is the ground silica glass for solutions A and B.

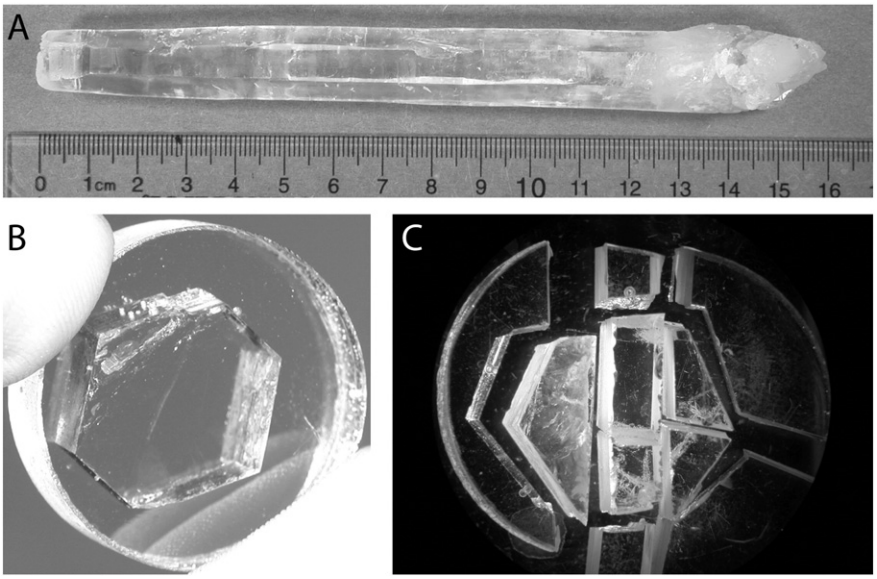

Fig. 3. Photographs of the quartz crystal used as a seed for experiments. (A) The crystal was 16 cm long and wafers were cut perpendicular to the C-axis. (B) Quartz wafer mounted in epoxy and polished using diamond suspension and colloidal alumina. (C) After polishing, the crystal was cut to provide multiple seed blocks. Seed blocks that had large fractures, visible scratches or apparent inclusions were not used.

quartz and to determine crystallographic orientation of both phases. Samples were then coated with a conductive layer of carbon and imaged by cathodoluminescence (CL), SE and BSE under high-vacuum SEM. The ground-glass starting material and the powders removed from the reaction vessels were analyzed by X-ray diffraction (XRD) to determine the phases present.

2.3. Isotope analysis of solid material

2.3.1. Secondary ionization mass spectrometer (SIMS) analysis of quartz

The $\delta^{18}O$ and $\delta^{30}Si$ values of diagenetic, detrital, seed, and experimentally precipitated quartz were measured using the CAMECA ims-1280 secondary ion mass spectrometer (SIMS) at the WiscSIMS Laboratory, University of Wisconsin-Madison (Kita et al., 2009; Valley and Kita, 2009; Heck et al., 2011). Both oxygen and silicon isotope ratios were analyzed using a primary beam of $^{133}Cs^+$ ions focused to a spot of ~10 μm diameter. Analysis pits were 1–2 μm deep.

Different analytical settings were used for oxygen and silicon isotope analyses. A 1.6 nA $^{133}Cs^+$ primary beam with a spot size of ~10 μm was used for $\delta^{18}O$ measurements. Ions of $^{16}O^-$ and $^{18}O^-$ were simultaneously collected in two movable Faraday cup detectors with an average $^{16}O^-$ intensity of 2.7×10^9 cps and $^{16}O^1H^-$ was collected in the axial Faraday cup to check for traces of water in quartz. A 2.2 nA $^{133}Cs^+$ primary beam with a spot size of ~10 μm was used for $\delta^{30}Si$ measurements. Ions of $^{28}Si^-$ and $^{30}Si^-$ were simultaneously collected in two Faraday cup detectors with an average $^{30}Si^-$ intensity of 1.2×10^8 cps. The magnetic field strength was held stable using a nuclear magnetic resonance (NMR) probe, which was readjusted every 12 h. The mass resolving power (MRP = M/ΔM), measured at 10% peak height, for $\delta^{18}O$ and $\delta^{30}Si$ analytical conditions was ~2200 for the movable Faraday detectors and ~5000 for the axial position, allowing $^{16}O^1H^-$ to be resolved from $^{17}O^-$ (Kita et al., 2009). Each spot analysis took approximately 4 min, which includes 10 s of presputtering to penetrate the carbon coat, ~60 s to stabilize sputtering and automatically center the secondary ions in the field aperture and 80 s (20 cycles of 4 s each) of integrating secondary ions. Detailed descriptions of these analytical conditions and the instrument setup at WiscSIMS have been published previously (Kelly et al., 2007; Kita et al., 2009; Valley and Kita, 2009; Heck et al., 2011; Wang et al., 2014).

All data were collected with a standard-sample-standard bracketing procedure of four UWQ-1 standard measurements, 10–16 sample measurements and four UWQ-1 standard measurements. Bracketing standards were used to evaluate the reproducibility of a series of measurements as well as to correct for the instrumental bias and minor instrument drift. The external spot-to-spot reproducibility of bracketing standards averaged ±0.22‰ (2SD) for oxygen isotope analyses and ±0.26‰ (2SD) for silicon isotope analyses. Raw values of isotope ratios measured by SIMS were corrected to the VSMOW scale for oxygen and the NBS-28 scale for silicon based on values measured for the UWQ-1 bracketing standards (UWQ-1: $\delta^{18}O = 12.33‰$, $\delta^{30}Si = -0.03‰$, Kelly et al., 2007; Heck et al., 2011). The best precision and accuracy is achieved in ims-1280 analyses that are within 5 mm of the center of a polished 25 mm mount (Kita et al., 2009; Peres et al., 2013). The wafer of seed quartz for experiment 250-2 cast in epoxy for SIMS analysis was larger than 10 mm, so only data from the overgrowth of one polished face (surface 1) of the wafer was used.

2.3.2. Laser fluorination analysis of $\delta^{18}O$ in powders

The powders from experiments with solutions A and B, as well as the ground-glass starting material, were analyzed for $\delta^{18}O$ by laser fluorination on a Finnigan/MAT 251 gas-source mass spectrometer in the Stable Isotope Laboratory, Department of Geoscience, University of Wisconsin, Madison using the rapid-heating, laser-fluorination technique of Spicuzza et al. (1998a) and a special air-lock sample chamber for the analysis of powders (Spicuzza et al., 1998b). UWG-2 garnet standard was measured 7–8 times during each analytical session and used to correct results to the VSMOW scale as outlined in Valley et al. (1995).

2.4. Isotope analysis of fluids

2.4.1. $\delta^{18}O$ analysis of fluids

The fluids to be analyzed for $\delta^{18}O$ were prepared and analyzed by direct fluorination following methods similar to those first described by O'Neil and Epstein (1966) and modified by Jabeen and Kusakabe (1997); Barkan and Luz (2005) and Kusakabe and Matsuhisa (2008). Nickel reaction vessels were attached to a manifold and pumped to high vacuum. Glass capillary tubes holding the water samples (3–5 μl per sample) were attached to the same vacuum line and cracked under vacuum to liberate the sample. The sample was then quantitatively transferred by heating the capillary tube and simultaneously cooling the Ni-reaction vessel with liquid nitrogen. An excess of BrF_5 (~1000 μmoles) was introduced to the reaction vessel and isolated

from the vacuum line. The Ni-reaction vessel was then heated to 230 °C for 45 min to liberate O_2. The O_2 was cryogenically purified, converted to CO_2 by reaction with a hot carbon rod, and analyzed on a Finnigan/MAT 251 gas source mass spectrometer.

The fluorination of water, as opposed to a more traditional equilibration with CO_2 (Epstein and Mayeda, 1953; Craig, 1957), is necessary due to 1) the small volumes of water available (3–5 μl per aliquot) and 2) the possible effects of dissolved NaOH, NaCl and $H_3SiO_4^-$ on the fractionation between H_2O and CO_2 during equilibration. The amount of oxygen in H_2O compared to H_xSiO_4 phases in solution in these experiments is large ($O(H_2O)$ / $O(H_xSiO_4)$ = 230) and does not change during the experiments. Thus, the $\delta^{18}O$ value measured is a true representation of the $\delta^{18}O$ of the fluid during the experiment. Measurements of $\delta^{18}O(H_2O)$ were performed for the starting and final fluids in all experiments in which quartz was precipitated. The precision of multiple measurements of $\delta^{18}O$ by this method was 0.12‰ 2SD. Within the period of analyses of unknowns, replicate samples of SMOW and SLAP were also measured. Data for unknowns were then calculated on both the VSMOW and VSMOW-SLAP scales. For comparison between solid and liquid, VSMOW values of $\delta^{18}O(H_2O)$ are used. A diagram of the fluorination apparatus is included in the supplemental material (Supplemental Fig. S2).

2.4.2. $\delta^{30}Si$ analysis of fluids

The $\delta^{30}Si$ of fluids from experiments that precipitated quartz and their starting solutions was measured at Trent University following methods described by Georg et al. (2006). Solutions for $\delta^{30}Si$ measurements were diluted immediately following experiments. At Trent, they were passed through a chromatographic column to separate Si from the matrix for subsequent analysis for $\delta^{30}Si$ and [Si] on a Thermo Finnigan Neptune MC-ICP-MS. Samples were aspirated using a microconcentric 100 μl/min PFA nebulizer (Elemental Scientific Inc.) into an ApexQ sample introduction system (Elemental Scientific Inc.), operational Si backgrounds were <50 mV on mass ^{28}Si. To resolve polyatomic interferences on Si masses, the mass-spectrometer was operated in medium mass resolving power (M/ΔM ~4500 at 5% & 95% peak height). Replicate analyses of the standard BHVO-2 (Abraham et al., 2008; Zambardi and Poitrasson, 2011) were run at the beginning and end of the analysis session to monitor precision and accuracy. The precision on $\delta^{30}Si$ measurements by this method was 0.1‰ 2SD.

3. Results

3.1. Experimental growth of quartz

The three solutions used in these experiments resulted in different amounts of quartz precipitation. Solution A (ground glass, NaOH, NaCl) had the largest amount of precipitated quartz, with a maximum thickness of ~235 μm new quartz after 126 days (Table 1A, Fig. 4A–E). Overgrowths of quartz were precipitated on both (001) faces of the wafers in the two long-term solution A experiments (250-2 and 250-3). Solution C (sodium silicate solution) had considerably less growth, with a maximum thickness of 8 μm new quartz grown on the seed crystal after 126 days (Table 1A, Fig. 4F,G). This solution also had loose crystals of doubly terminated α-quartz ~50 μm in length, which precipitated in the solution and settled onto the wafer of seed quartz (Fig. 4H,I). Solution B (NaOH, ground glass) had no measurable growth on any seed crystal face, nor crystals precipitated in solution, even after the longest experimental time (126 days). All experimentally grown quartz that precipitated on the seed quartz crystals were confirmed by EBSD to be in the same crystallographic orientation as the seed (Fig. 4A).

In addition to quartz, some experiments were found to have precipitated trace amounts of analcime (Table 1A, Fig. 4H,J,K). The sodium necessary for this mineral was readily available from the NaOH, NaCl or sodium silicate in the solutions. The source of Al was initially puzzling, but it was found that a small amount of aluminum had been smeared onto some of the wafers of seed quartz from a flange on the saw used to cut them. The identification of analcime was confirmed by spot XRD analysis of individual ~100 μm crystals (Supplemental Fig. S3).

Powders from solutions A and B and the starting ground glass were analyzed by XRD. Peaks for crystalline quartz were observed in powders from experiments 250-2 and 250-3, but not in the starting glass, SG-1 (Fig. 5). A broad low-magnitude peak was observed at low 2θ in all three samples (SG-1, 250-2 and 250-3), which is consistent with glass (Fig. 5).

3.2. Isotope ratios of solids

3.2.1. $\delta^{18}O$ values of experimental quartz overgrowth and powders

Two experimental runs from this study (solution A, 86 and 126 days, 250-2 and 250-3, respectively) had >200 μm thick quartz precipitated as overgrowths on the seed crystal that were analyzed by SIMS for $\delta^{18}O$ (Tables 1B, ST1). The average for spots on newly grown quartz measured in surface 1 of 250-2 (closest to center of epoxy mount) is $\delta^{18}O = 4.27 \pm 0.06$‰ 2SE, n = 18. The average for all overgrowth spots from both faces measured in 250-3 is $\delta^{18}O = 4.07 \pm 0.06$‰ 2SE, n = 87 (Tables 1B, ST1).

In addition to the quartz precipitated on seed crystals, the experimental products using solutions A and B contained glass powder that was partially recrystallized to quartz, as confirmed by XRD. The percent recrystallization compared to the original glass was not determined. The $\delta^{18}O$ values of these powders, as well as the ground glass starting material, were measured by laser fluorination to determine whether the isotope ratios of powders in the solution were the same as the oriented quartz precipitated on the seed crystal and are reported in Tables 1A, 1B and 1C. The $\delta^{18}O$ of powder from 250 to 3 is the same within analytical uncertainty as values measured by SIMS for the quartz overgrowth (powder $\delta^{18}O = 4.30 \pm 0.21$‰, SIMS $\delta^{18}O = 4.07 \pm 0.06$‰). The $\delta^{18}O$ value of powder from 250 to 2 is higher than the SIMS value for new quartz overgrowths (7.3‰ vs. 4.3‰), suggesting a mixture of new quartz and starting ground glass ($\delta^{18}O = 9.94$‰). All SIMS $\delta^{18}O$ values for experiments are reported in supplemental Table ST1.

3.2.2. $\delta^{30}Si$ values of experimentally grown quartz

Quartz from the two long-term experiments using solution A (250-2, 250-3) was also analyzed for $\delta^{30}Si$ by SIMS. The average $\delta^{30}Si$ for overgrowth spots measured in surface 1 of 250-2 is 0.21 ± 0.14‰ 2SE, n = 16. The average for all spot analyses on overgrowths in 250-3 is $\delta^{30}Si = 0.43 \pm 0.06$‰ 2SE, n = 68. All SIMS $\delta^{30}Si$ values for experiments are reported in supplemental Table ST2.

Given the spatial resolution of the SIMS technique, it is possible to determine if the O or Si isotope values of the precipitated quartz varied over the course of the experiment. Analyses were conducted across the entire cross-section of precipitated quartz and no systematic variability was measured in either $\delta^{18}O$(quartz) or $\delta^{30}Si$(quartz).

3.3. Isotope values of fluids

3.3.1. $\delta^{18}O$ values of fluids

The $\delta^{18}O$ values of fluids from experiments that precipitated quartz overgrowths and the corresponding starting fluids were measured by fluorination (Tables 1B, 3). The $\delta^{18}O$ values of the solutions after the experiments are −6.5‰ and −8.5‰ for solutions A and C, respectively, and are ~0.5‰ and 0.3‰ higher in $\delta^{18}O$ than in the corresponding starting fluids.

3.3.2. $\delta^{30}Si$ values of fluids

The $\delta^{30}Si$ values of dissolved silicon in fluids from experiments that precipitated quartz overgrowths and the corresponding starting fluids were measured by MC-ICP-MS (Table 1C). The $\delta^{30}Si$(fluid) values of

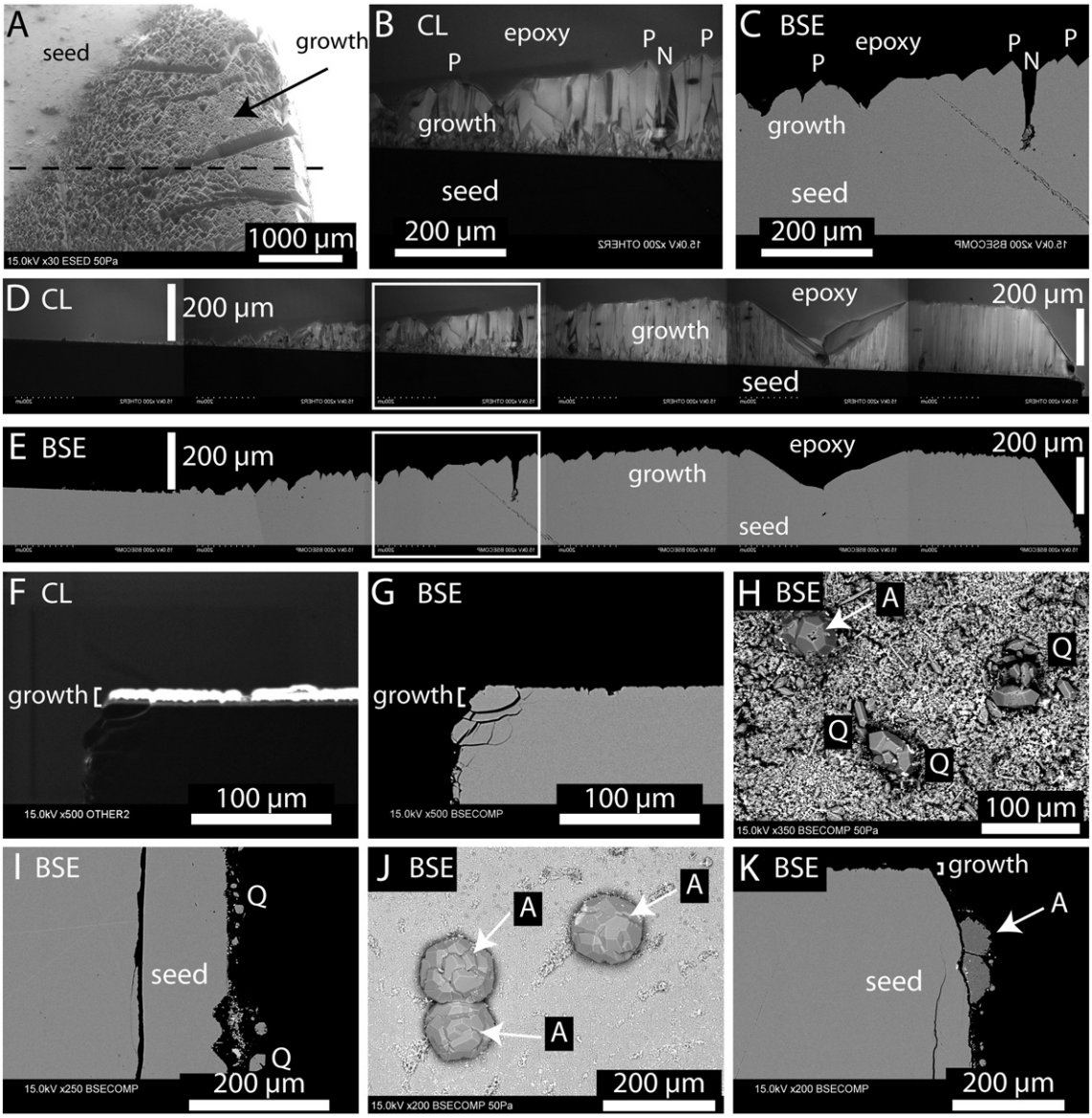

Fig. 4. SEM photomicrographs of experimentally precipitated quartz and analcime. (A) Experimentally precipitated quartz covers most of the seed quartz in experiment 250-3 (Solution A, 250 °C, 126 days). Flat area in upper left of image is a section of the original (001) surface of the seed crystal where no quartz precipitated. Note the many pyramidal terminations of quartz crystals with the same orientation, controlled by the orientation of the seed. The dashed line represents the cross-section shown in D and E. (B) and (C) Enlarged cathodoluminescence (CL) and backscattered electron (BSE) images of a polished cross-section of experiment 250-3 (box in D and E). The bright, experimentally grown quartz is distinguished by CL from the dark seed crystal. Notches (N) between quartz pyramidal terminations (P) appear to be controlled by "dust", which may be powder from the excess glass in starting material. (D) and (E) CL and BSE images of the full cross-section shown in A. The maximum thickness of the new quartz is 235 μm. (F) and (G) CL and BSE images of experiment 250-9 (Solution C, 250 °C, 126 days) polished cross-section. The seed crystal is distinguishable from the precipitated quartz in this image, but the thickness of new quartz is only 8 μm. F and G show only one corner of the seed crystal, but the growth is continuous across the entire (001) surface. (H) Phases precipitated in solution and on the polished face perpendicular to the C-axis of 250-9 showing doubly terminated quartz crystals (Q) and analcime (A). (I) BSE image of 250-9 polished cross-section. The seed crystal is present, but in this orientation no quartz overgrowth is seen. The crack ~100 μm deep in the seed is a fracture that occurred during cutting and mounting after the experiment. (J) Surface of 250-9 showing clusters of analcime crystals. (K) BSE image of 250-9 polished cross-section. A thin overgrowth in the same orientation as F and G is present in this image. Analcime crystals are slightly darker than quartz seed in BSE.

250-2 and 250-3 are −0.30 and −0.15‰, respectively. The δ^{30}Si(fluid) of experiment 250-9, which yielded quartz overgrowths too thin for SIMS analysis, is 0.22‰. The δ^{30}Si of the starting solutions A and C are 0.06 and 0.27‰, respectively.

4. Discussion

4.1. Quartz growth rates

It is clear from the variable amounts of quartz precipitated in the different experiments of this study that solution chemistry has a major impact on the growth rate of quartz. Growth rates in previous studies are often reported as moles/cm^{2}s (e.g., Walderhaug, 1994; Lander et al., 2008). Given the availability of cross-sections of experimental quartz in this study, we report our findings in both μm/day (linear growth rate) and moles/cm^{2}s for comparison to previous studies. Over the time scale of these experiments (maximum of 126 days), growth from a solution of ground glass and NaOH (solution B) is not observable (new quartz growth was not observed by SEM, and is therefore either not present, or is significantly less than 1 μm). This is in sharp contrast to the quartz growth rates measured in experiments containing a solution of ground glass, NaOH and NaCl (solution A), where growth rates were as high as 1.9 μm/day (9.5×10^{-11} mol/cm^{2}s). The fast growth rates measured in solution A are similar to rates reported in other quartz precipitation experiments (Mackenzie and Gees, 1971; Lander et al., 2008) and are approximately six orders of magnitude

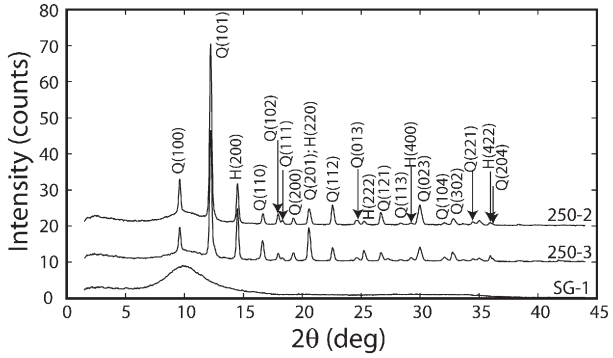

Fig. 5. Powder X-ray diffraction patterns for silica glass (SG-1) starting material and powders removed from experiments. Peaks are labeled for crystallographic planes in alpha-quartz (Q) and halite (H); all identified peaks are for these two minerals, but for clarity not all peaks are labeled. Note broad peak at low 2θ for SG-1 showing presence of glass as well as lack of sharp diffraction peaks. 250-2 and 250-3 are experimental products from solution A with NaCl. A broad peak is present in the background of the experimental data, but it is much lower magnitude than for the starting glass. Patterns are vertically offset from each other, but have the same vertical scale.

faster than rates estimated for naturally precipitated quartz (Fig. 6; Walderhaug, 1994). Walderhaug (1994) made the assumption that the growth of quartz is a continuous process, leading to a possible overestimation of the total duration of precipitation and a corresponding lowering of the growth rate; however, this is just one possible explanation for this large difference in growth rate. Solutions that are used in experimental precipitation of quartz often have salt, pH, and [Si] values far from what may be expected in nature; this may also contribute to the significant differences in growth rates estimated from experiments vs. natural quartz. This question is reviewed by Worden and Morad (2000). Dove (1994)interpreted fast dissolution rates of quartz in solutions with dissolved salts to be due to solvation shells around dissolved species, which can affect the orientation of the oxygen atoms of the Si-O

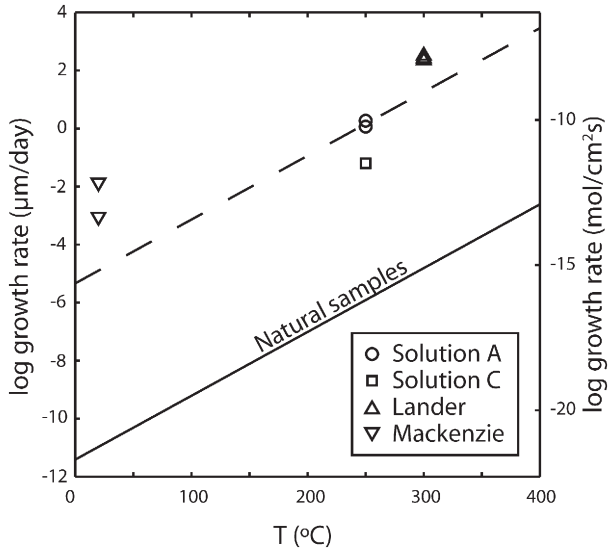

Fig. 6. Comparison of quartz growth rates estimated from natural samples (Walderhaug, 1994) and experimentally precipitated quartz (this study; Mackenzie and Gees, 1971; Lander et al., 2008) as a function of temperature. Solutions A and C are from this study. Values for Mackenzie and Gees (1971) are the maximum rate commonly cited from that study (10 μm grown in 2 years) as well as the minimum rate estimated from photographs from that study (1 μm in 3 years). Growth rates for experiments are up to six orders of magnitude higher than those estimated from natural samples. The dashed line follows the slope of the Walderhaug (1994) calibration, but is offset to pass through the results of this study. It can be seen from this fit that even though the growth rates measured in the present study are faster than rates estimated from natural samples, they are relatively slow in relation to other experiments. See Section 4.1 for discussion.

lattice. A similar process may be the cause of the rapid growth rates in NaCl solutions.

4.2. Recrystallization of glass powders

In addition to the quartz that was precipitated as overgrowths in three of the reaction vessels, extra ground glass that was placed into the vessels (to continuously supply silicon to the fluids) crystallized to quartz during the runs, as seen in XRD patterns (Fig. 5). The XRD measurements were made with powder packed into glass capillaries, so some of the broad glass signal observed for starting materials and products is from the capillary tube. Still, it is clear that the experimental products contain sharp quartz diffraction peaks, whereas the starting glass does not (Fig. 5), indicating that a significant amount of quartz crystallized from the powder during these experiments.

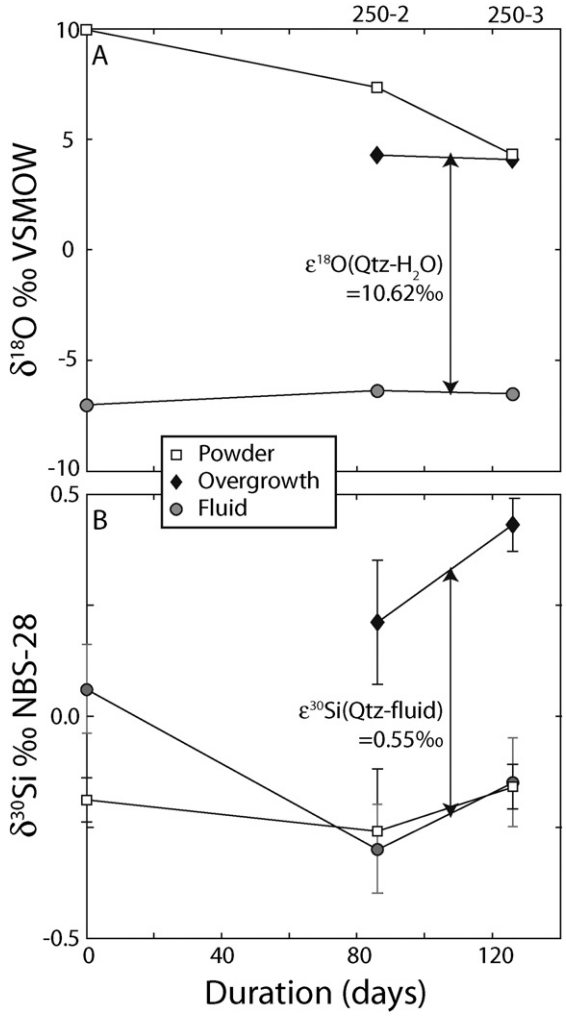

Fig. 7. Isotope composition of experimental products and starting material from solution A as a function of experiment duration showing (A) oxygen isotope composition and (B) silicon isotope composition. Values at 0 days are the $\delta^{18}O$ and $\delta^{30}Si$ of starting powder and solution A. Numbers above the top X-axis are experiment numbers. Overgrowth $\delta^{18}O$ and $\delta^{30}Si$ are the values measured by SIMS; the difference between this and $\delta^{18}O(H_2O)$ or $\delta^{30}Si$(fluid) respectively reflects the equilibrium fractionation between quartz and water ($\varepsilon^{18}O = 10.62 \pm 0.13‰$; $\varepsilon^{30}Si = 0.55 \pm 0.10‰$ for these experiments). (A) The $\delta^{18}O$ of powder from experiment 250-2 shows incomplete reaction; the powder in 250-3 has fully reacted. Note 2 SD uncertainties are smaller than symbols. (B) The $\delta^{30}Si$ of the powder is constant, representing exchange in a local environment isolated from the bulk of the solution; see Section 4.4 for discussion. Error bars represent 2 SD uncertainties; note expanded scale of Y-axis in panel B as compared to the scale in panel A.

4.3. $\delta^{18}O$ values of powders

The similarity between the $\delta^{18}O$ of quartz overgrowths and the final powder in 250-3 (4.07‰ vs. 4.30‰ respectively; Fig. 7A) suggests that both generations of quartz fully exchanged with the solutions and that the powders may also be used in determining the quartz–water fractionation factors for experiments that produced no measurable quartz overgrowths. However it is possible that some of the original ground glass may remain unexchanged in the powdered samples, which would bias the measured values away from equilibrium precipitation.

The powder from experiment 250-2 (same starting solution as 250-3) has a $\delta^{18}O$ of 7.34‰, ~3‰ higher than the quartz measured by SIMS from the same experiment (Fig. 7A). Experiment 250-2 was heated for 86 days, as compared to 250-3, which was heated for 126 days. The ground glass, which was included in solutions A and B, has a $\delta^{18}O$ value of 9.94‰. The fact that the powder from experiment 250-2 has a $\delta^{18}O$ value that is intermediate between the precipitated quartz and the starting material, suggests that this experiment, which ran for a shorter amount of time, has a higher proportion of unreacted starting glass included in the bulk powder. This underlines the importance of analyzing the isotope ratios in situ for solid materials, which can be imaged and shown to be precipitated during the experiment. Even fine-grained (<10 μm) silica glass in an experiment for 86 days at 250 °C did not fully exchange with the fluid (Fig. 7A). In contrast, the powder in experiment 250-3 does appear to have fully exchanged in 126 days, although this would be unknown if the quartz overgrowth was not analyzed for confirmation.

4.4. $\delta^{30}Si$ values of powders

The data for $\delta^{18}O$ in Fig. 7A clearly show that the excess powder included in the reaction vessels was exchanging over the course of the experiment and suggests that experiment 250-3 achieved isotopic equilibrium with respect to oxygen. However, a similar plot for $\delta^{30}Si$ (Fig. 7B) suggests a potentially different process dominated Si exchange compared to O. In these experiments the dominant source of O for the quartz forming reaction is the 0.1 M NaOH solution (which consists primarily of H_2O) and the dominant source of Si is the Si in solution, which is in turn sourced from the starting glass SG-1 both prior to the experiment, and the excess ground silica powder (also SG-1) in the reaction vessel. Due to the experiment design, the fluids were not stirred in the vessels during the course of the experiments, so it is possible that small-scale chemical heterogeneities existed between different parts of the reaction vessel. This is primarily a concern in the pore spaces within the fine-grained powder resting on the bottom of the vessel. Because the reservoir for O in these experiments is large compared to that for Si, it is expected that the effect will be magnified for Si.

The seed crystal in the experiments was much larger than the pile of powder, so the faces where new quartz precipitated were fully exposed and interacted directly with the fluid. However, the crystallization of quartz in the powder (which is confirmed by XRD; Fig. 5) occurred in a partially closed system with respect to $\delta^{30}Si$. If the powder dissolved and reprecipitated in a closed system but the quartz overgrowth grew from a fluid that was changing over time, this may explain the apparently constant $\delta^{30}Si$(powder) and varying $\delta^{30}Si$(fluid) and $\delta^{30}Si$(overgrowth) values in Fig. 7B. It should be noted that although this figure appears to reflect wide variability in measured values, the scale is significantly expanded compared to $\delta^{18}O$. There is no significant variability between any $\delta^{30}Si$ values from these experiments, and indeed most of the powder and fluid values are within uncertainty of each other.

4.5. $\delta^{18}O$ values of starting and ending fluids

The ~0.5‰ increase in $\delta^{18}O$ from starting to ending liquids (Table 1B) may be due to minor corrosion of the stainless steel vessel with the vapor phase (observed as slight discoloration of the interior of the vessels after opening), minor evaporation and condensation between the liner and vessel either during the experiment or during quenching, or the precipitation of quartz. The fact that the $\delta^{18}O$ and $\delta^{30}Si$ of precipitated quartz does not vary systematically from early to late quartz suggests that the isotopic values of the fluid did not change during quartz precipitation. The minor discoloration of the interiors of reaction vessels is likely due to oxidation of the stainless steel, which occurred rapidly upon initial heating of the vessels. The small shift in $\delta^{18}O(H_2O)$ during the experiment had little effect on the calculation of fractionation factors. The important phases for fractionation calibration are the final quartz and final fluid.

4.6. Quartz–water fractionation

4.6.1. $\varepsilon^{18}O(Qtz–H_2O)$

The data from experimentally precipitated quartz overgrowths in two reaction vessels can be used to calculate the equilibrium fractionation factor between quartz and water at 250 °C. Experiments 250-2 and 250-3 are in excellent agreement with an average value of $\varepsilon^{18}O(Qtz–H_2O) \approx 1000\ln\alpha^{18}O(Qtz–H_2O) = 10.62 \pm 0.13‰$ ($10.64 \pm 0.10‰$ and $10.59 \pm 0.23‰$ 2SD, for 250-2 and 250-3 respectively; Fig. 7A, Supplemental Fig. S4).

As seen in Fig. 1, there are large differences between calibrations of $1000\ln\alpha^{18}O(Qtz–H_2O)$ vs. temperature from different studies. The value of 10.6‰ for $\varepsilon^{18}O(Qtz–H_2O)$ measured in this study at 250 °C is within uncertainty of one and just outside uncertainty of a second previously published calibration (10.61‰, Shiro and Sakai, 1972; 10.44‰, Sharp and Kirschner, 1994; Supplemental Fig. S4), even though pH and dissolved content of the present study and previous studies are likely quite different.

4.6.2. $\varepsilon^{30}Si(Qtz–fluid)$

There are no previous experimental calibrations for silicon isotope fractionation between quartz and an aqueous solution. Estimates exist for $\varepsilon^{30}Si$(silica–fluid) based on: empirical studies of quartz (Douthitt, 1982); measurements of natural and experimentally precipitated biogenic silica from sponges or diatoms (Douthitt, 1982; De La Rocha et al., 1997; De La Rocha, 2003); or experimentally precipitated silica gel (Li et al., 1995) and amorphous silica (Geilert et al., 2014; Roerdink et al., 2015). Experiments have also been performed to measure the Si fractionation during adsorption of silica onto various hydroxide and oxyhydroxide phases (ferrihydrite and goethite, Delstanche et al., 2009; gibbsite, Oelze et al., 2014) and formation of Fe-Si gels (Reddy et al., 2015; Zheng et al., 2015), but since the processes that control fractionation during sorption onto hydroxides or formation of gels are likely to be different from those during mineral precipitation and growth, these calibrations are not considered further here.

Two recent studies measured the $\delta^{30}Si$ of starting and final fluids after they had passed through a flow reactor and estimated the fractionation assuming that the difference is due to the precipitation of amorphous silica (Geilert et al., 2014; Roerdink et al., 2015). The $\varepsilon^{30}Si$(silica–fluid) values from Geilert et al. (2014) vary from 0.2‰ at 60 °C to −2.1‰ at 10 °C. The authors of that study conclude that 1) the values measured in their study reproduce values measured in previous studies and 2) their values do not represent equilibrium fractionation; which led to the interpretation that previous experimental and empirical calibrations of Si fractionation represent kinetic rather than equilibrium fractionation (Geilert et al., 2014). Roerdink et al. (2015) interpreted results from their experiments as being dominated by kinetic fractionation during the early time steps with a metastable state being approached later during the experiment. The $\varepsilon^{30}Si$(silica–fluid) values presented as kinetic in that study range from −0.7‰ at 35 °C to −3.5‰ at 10 °C and those interpreted as metastable range from 0.5‰ at 35 °C to −0.5‰ at 10 °C (Roerdink et al., 2015).

Recent calculations of the fractionation of silicon isotopes between quartz and fluid, and between different silica species in solutions (e.g., $H_3SiO_4^-$ vs. H_4SiO_4) suggest that the bonding of silicon in different aqueous molecules may have a large, previously unrecognized effect on equilibrium fractionation (Méheut and Schauble, 2014; Dupuis et al., 2015; Méheut, personal communication). These first-principles density function and phonon frequency calculations yield positive ε^{30}Si values for the fractionation between quartz and $H_3SiO_4^-$, similar to that measured experimentally in this study. Dupuis et al. (2015) presented values of $\varepsilon^{30}Si(Qtz–H_4SiO_4) = 2.09 \pm 0.13‰$ and $\varepsilon^{30}Si(Qtz–H_3SiO_4^-) = 3.69 \pm 0.10‰$ at 300 K.

The ε^{30}Si(Qtz–fluid) values for experiments 250-2 and 250-3 from the present study are in excellent agreement (0.51‰ and 0.58‰, respectively) and average 0.55 ± 0.10‰ (Fig. 7B). If extended to lower temperatures, these values are between 1 to 7‰ higher than previously published experimental and empirical estimates (Fig. 8).

The results of this study agree well with recent calculations of silicon fractionation, but are significantly different from previous experimental and empirical estimates. Dupuis et al. (2015) suggested that the discrepancy between their positive calculated ε^{30}Si values and all previous estimates is that precipitation of silica at low temperatures in natural settings is out of equilibrium with respect to silicon isotopes. Additionally, no previous studies have reported values for abiogenic quartz and fluid from the same locations. The majority of ε^{30}Si values published are based either on biogenic silica from diatoms and sponges where vital effects are unknown but may be large, or from experimentally precipitated amorphous silica, which is significantly different from quartz.

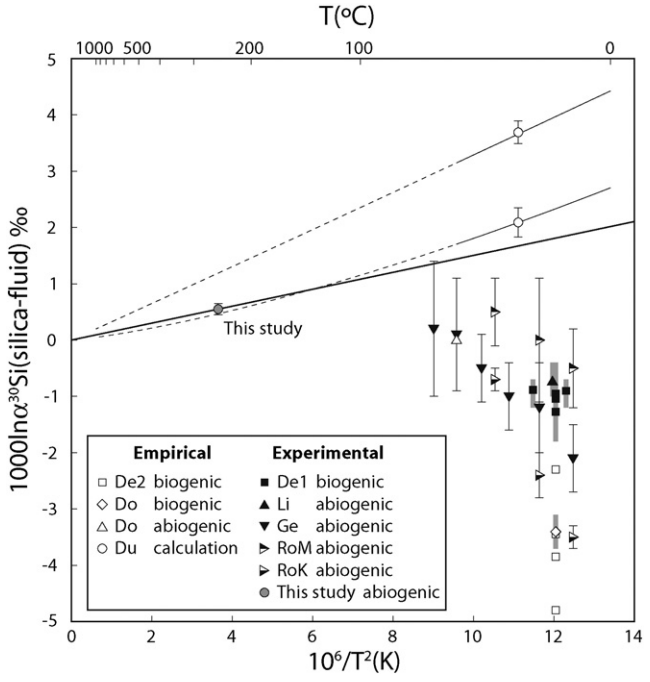

Fig. 8. Comparison of estimates of silica–fluid and quartz–fluid silicon isotope fractionation factors at low temperatures. There is a large range of values; many are empirical or for biogenic silica. See Section 4.6.2 for discussion. Error bars on individual points are 2SD for this study, Geilert et al. (2014), & Roerdink et al. (2015), and 2SE for Dupuis et al. (2015). Thick vertical bars represent the range of values measured in given studies. Thick black line is fit through experimental data of this study and 0‰ at infinite temperature. All biogenic experimental data are based on cultured diatoms from De La Rocha et al. (1997), black squares); all biogenic empirical data are based on sponges from De La Rocha (2003), open squares) except one estimate from biogenic opal from Douthitt (1982, open diamond). Experimental abiogenic points are shown as a black triangle with a thick bar at 15 °C (Li et al., 1995), inverted black triangles over a range of temperatures with error bars (Geilert et al., 2014), and right pointing triangles over a range of temperatures with error bars (Roerdink et al., 2015). Open circles are calculations of Dupuis et al. (2015) based on phonon frequencies and represent $1000ln\alpha^{30}Si(Qtz–H_3SiO_4^-) = 3.69$ and $1000ln\alpha^{30}Si(Qtz–H_4SiO_4) = 2.09$; at the pH of experiments in the present study (pH ≈ 12), the dominant species was $H_3SiO_4^-$, with minor $H_2SiO_4^{2-}$. Curves that pass through the open circles are temperature dependent fits calculated in Dupuis et al. (2015) for $1000ln\alpha^{30}Si(Qtz–H_3SiO_4^-)$ and $1000ln\alpha^{30}Si(Qtz–H_4SiO_4)$; curves are solid over the temperature range reported in the previous study (0–50 °C) and dashed where extrapolated (50–1000 °C). The abbreviations are: De1 = De La Rocha et al. (1997); De2 = De La Rocha (2003); Do = Douthitt (1982); Du = Dupuis et al. (2015); Li = Li et al. (1995); Ge = Geilert et al. (2014); RoM = metastable values from Roerdink et al. (2015); RoK = kinetic values from Roerdink et al. (2015).

The close agreement at 250 °C between the experiments in this study and recent calculations for H_4SiO_4 and $H_3SiO_4^-$ molecules (0.08‰ lower and 0.64‰ higher respectively than the current experiments) suggest that the values measured here represent equilibrium fractionation between quartz and dissolved silica. The dominant silica species at the pH of the experiments in this study was $H_3SiO_4^-$ calculated using the geochemical code PHREEQC with the Lawrence Livermore National Laboratory thermodynamic database (G. Saldi, personal communication). The fractionation between $H_3SiO_4^-$ and H_4SiO_4 presented by Dupuis et al. (2015) is −1.6‰ at 27 °C and −0.52‰ when extrapolated to 250 °C. Applying this value to the ε^{30}Si(Qtz–fluid) of +0.55‰ measured in the experiments of this study will lower the value to 0.03‰, which is significantly higher than the ~ − 1.5‰ value that has been reported in previous studies (Fig. 8). It is likely that previous experiments did not attain isotopic equilibrium, perhaps due to low temperatures, circumneutral pH and low Si concentrations, which is supported by the conclusions of Geilert et al. (2014), or that the fractionation between amorphous silica and fluid is significantly different from that between quartz and fluid.

4.7. Application of experimental $\varepsilon^{18}O(Qtz–H_2O)$ and $\varepsilon^{30}Si(Qtz–fluid)$ calibration to natural samples

Interpretations of silicon isotope data from natural samples have been hampered by the uncertainty of fractionation factors for quartz. Despite this ambiguity, there is significant interest in the ability to measure δ^{30}Si(Qtz) from many sample types (e.g., Basile-Doelsch, 2006; Georg et al., 2009; Heck et al., 2011). In particular, new SIMS protocols allow accurate analysis of diagenetic quartz overgrowths and can be used for interpreting the dissolved components, and thus the sources and pathways of fluid flow. Given the large range in previously published ε^{30}Si(Qtz–fluid) values, and the significant difference between those values and the results of this study, it is possible that diagenetic quartz precipitation in nature is often a non-equilibrium process and that the controls on fractionation of silicon isotopes are significantly different.

4.7.1. Geologic background and sample localities

The Mt. Simon Sandstone (Ss) is a texturally mature feldspathic or subfeldspathic arenite (Hoholick et al., 1984), which unconformably overlies the Precambrian basement across much of the mid-continent of North America from Nebraska to Ohio and from Kentucky to Minnesota. The majority of the formation was deposited in a marine setting (Willman et al., 1975), while the lower sections contain alluvial, coastal and tidal deposits and are more feldspathic than the upper part (Templeton, 1951; Buschbach, 1964). The Mt. Simon ranges in thickness in the Illinois Basin from less than 91 m to 792 m (Hoholick et al., 1984), reaches a maximum current burial depth of ~4500 m in southern Illinois, and outcrops in Wisconsin where the dip is gentle and to the southeast. The Mt. Simon in the Illinois Basin has been interpreted to have been buried up to 1 km deeper than its current depth; whereas sections currently exposed in Wisconsin experienced less burial and uplift (Mai and Dott, 1985). The differences in maximum burial have led to significant differences in the hydrologic and thermal histories of Paleozoic sediments in the Illinois Basin vs. on the Wisconsin Dome and Arch (e.g., Kelly et al., 2007; Pollington et al., 2011; Hyodo et al., 2014).

The Mt. Simon Ss has been the subject of numerous studies to describe and interpret its depositional and cementation histories

(e.g., Driese, 1979; Hoholick et al., 1984; Chen et al., 2001; Bowen et al., 2011; Pollington et al., 2011; Leetaru and Freiburg, 2014). The dominant diagenetic cements are syntaxial quartz overgrowths on detrital quartz grains, with feldspar overgrowths common where detrital feldspar is present, as well as some interstitial clays & iron oxides and rarely carbonates. Regionally, quartz overgrowths are distributed throughout the formation. However, at the centimeter to meter scale, there can be large differences in cement distribution resulting in porosity that ranges from 1% to 40% even in the same depth interval (Bowen et al., 2011; Pollington et al., 2011). This difference in porosity may be caused by slight variability in primary textures due to differences in depositional environment, as well as secondary porosity (Bowen et al., 2011).

The samples analyzed in this study were collected from drill cores in Illinois and outcrops in Wisconsin and span a north to south traverse of 680 km (Table 2; Fig. 9). Samples from drill core are from the north, central, and southern parts of Illinois and cover present-day depth ranges of 394–664 m, 1648–1982 m and 2579–2581 m respectively. Samples from outcrops can be divided into two broad groups: four samples are from two nearby outcrops in central Wisconsin (outcrop set A); and nine samples are from five outcrops from a wider range of central Wisconsin (outcrop set B). The outcrops in set A are stratigraphically a few meters above the Precambrian-Cambrian unconformity although the contact is not exposed at these localities. Two outcrops from set B expose the unconformity and samples from those outcrops were from within 0.5 m of the contact.

4.7.2. Sandstone characterization

Detrital quartz grains (DQ) and overgrowth quartz cements (OQ) in samples of Mt. Simon Ss were identified by SEM-CL in thin sections and ~1 cm^3 chips mounted in epoxy. Multiple generations of cement are present in samples from outcrop set A and are distinguishable by different CL response (Fig. 10). There is an early, bright-CL, concentrically banded domain (Q1) present in many overgrowths from set A followed by a second dark-CL domain that is present in all overgrowths and represents the majority of OQ from the samples of outcrop set A. In two overgrowths that were analyzed for $\delta^{18}O$ and $\delta^{30}Si$, there is a third, final generation (Q3) of bright CL OQ near the overgrowth boundary. The Q2 domain is observed in all overgrowths from outcrop set A, but Q1 and Q3 are present in a much smaller subset of overgrowth quartz. No single overgrowth contains all three generations of cement. Overgrowths from outcrop set B and drill cores from the Illinois Basin tend to not have systematic CL zonation like that observed in outcrop set A.

Table 2
Locations of Mt. Simon sandstone samples used in this study.

Sample ID	Drill core number[a]	Outcrop set or current burial depth (m)	Latitude N	Longitude W
Drill cores				
09IL-1	12,996	434.52	42.437308	−89.857855
09IL-6	12,996	434.52	42.437308	−89.857855
09IL-29	12,996	663.42	42.437308	−89.857855
09IL-31	13,639	1648.36	40.127100	−87.559575
09IL-33	13,639	1652.63	40.127100	−87.559575
09IL-35	13,639	1875.89	40.127100	−87.559575
09IL-39	13,639	1980.90	40.127100	−87.559575
09IL-41	13,639	1982.11	40.127100	−87.559575
09IL-46	4831	2579.37	38.552155	−89.022456
09IL-50	4831	2581.28	38.552155	−89.022456
Outcrops				
07WI-1[b]	–	A	–	–
09WI-2	–	B	44.358066	−90.792633
09WI-10	–	B	44.551566	−90.657933
09WI-13	–	B	44.559866	−90.612683
09WI-14	–	B	44.449433	−89.827383
09WI-15	–	B	44.449433	−89.827383
09WI-16	–	B	44.449433	−89.827383
09WI-17	–	A	44.473283	−89.647650
09WI-18	–	A	44.473283	−89.647650
09WI-21	–	B	43.930150	−89.803950

[a] All drill core numbers are Illinois State Geological Survey core ID numbers.
[b] Sample 07WI-1 was collected by Prof. R. Dott, Jr. The hand sample was cut into two pieces, 07WI-1L and 07WI-1D based on the dominant banding (light and dark). The sampling location is approximate and between samples 09WI-14,-15,-16 and 09WI-17,-18.

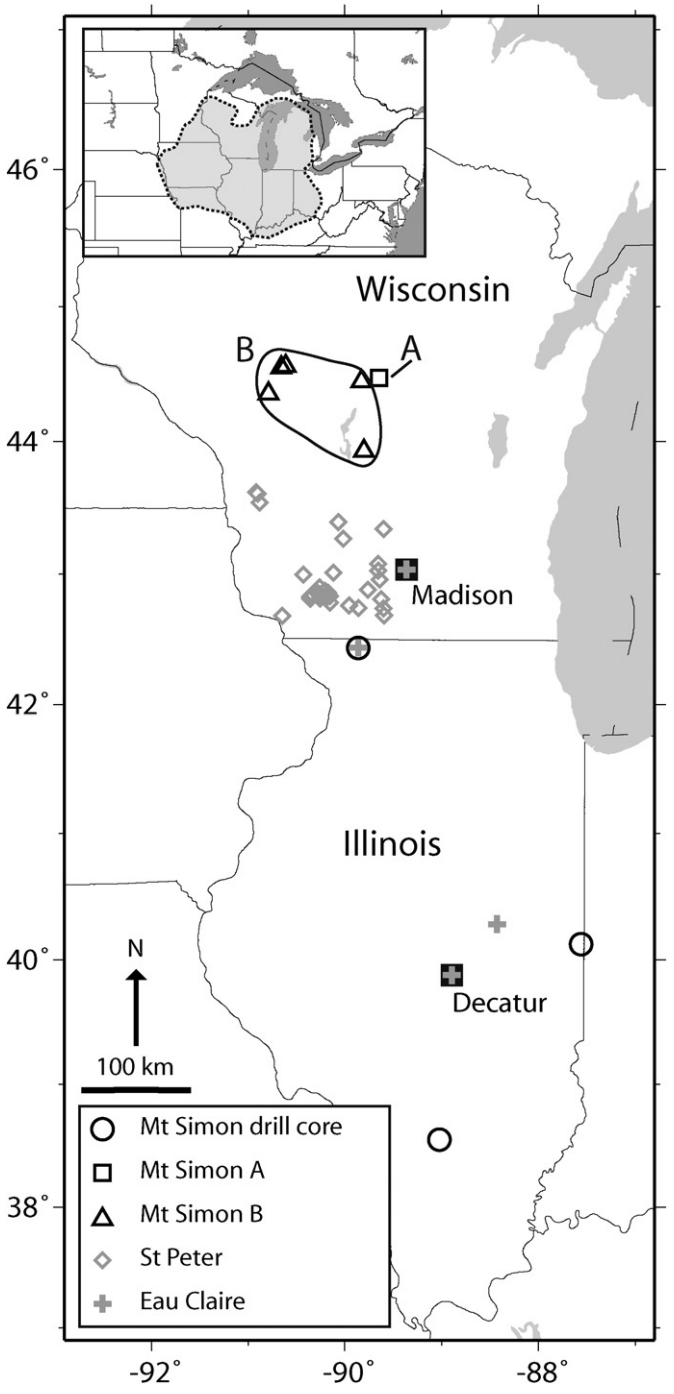

Fig. 9. Map showing sample locations in Wisconsin and Illinois. Circles represent Mt. Simon Ss in drill core, open square represents outcrop set A (see Section 4.7.1), triangles represent outcrop set B, diamonds represent samples from the St. Peter Ss (Kelly et al., 2007), crosses represent drill core samples of the Eau Claire Formation (Hyodo et al., 2014). Data reported in the present study are from all Mt. Simon locations shown. Inset shows the approximate extent of the Mt. Simon Ss throughout North America.

4.7.3. $\delta^{18}O$ and $\delta^{30}Si$ values of sandstone samples

Oxygen isotope values of detrital quartz average $\delta^{18}O(DQ) = 9.7 \pm 4.2‰$ (2SD, n = 72) from outcrops of the Mt. Simon Ss and are similar to

Table 3
Values of $\delta^{18}O(H_2O)$ for experimental products & starting fluids, and standards measured by fluorination of water and gas-source mass spectrometry.

Analysis no.	Sample no.[a]	µl[b]	% yield	$\delta^{18}O$ raw	$\delta^{18}O$ VSMOW[c]	$\delta^{18}O$ VSMOW-SLAP[d]
FW-						
120-1	UWDW-2	5	102.8	−8.93	−9.08	−9.20
120-3	250-3	6	98.6	−6.24	−6.39	−6.48
120-4	250-2	6	100.1	−6.25	−6.40	−6.49
122-1	UWDW-2	5	103.3	−8.88	−9.03	−9.15
122-2	250-2	6	102.0	−6.19	−6.34	−6.43
122-3	A before	6	108.0	−6.80	−6.95	−7.04
122-4	250-9	6	110.4	−8.39	−8.54	−8.66
124-1	UWDW-2	5	102.6	−9.03	−9.18	−9.30
124-2	250-3a	5	101.3	−6.45	−6.60	−6.69
124-3	250-9	6	105.2	−8.27	−8.42	−8.53
126-1	UWDW-2	5	99.2	−8.90	−9.05	−9.17
126-2	250-3a	5	101.3	−6.41	−6.56	−6.65
126-3	A after	6	95.7	−6.94	−7.09	−7.19
126-4	C before	6	97.3	−8.68	−8.83	−8.95
128-1	UWDW-2	5	102.8	−8.95	−9.10	−9.22
128-2	C before	9	99.7	−8.56	−8.71	−8.83
128-3	SMOW	5	100.5	0.08	−0.07	−0.07
130-1	SMOW	5	100.0	0.08	−0.07	−0.07
130-2	SMOW	5	99.5	0.28	0.13	0.13
130-3	SLAP	5	103.5	−54.48	−54.63	−55.37
130-4	SLAP	5	101.8	−54.73	−54.88	−55.63

SMOW and SLAP samples were sealed in 5 µl glass capillaries in 1994 and stored at UW-Madison. Measured values confirm that there was no exchange of these samples over the past 19 years.
Precision is 0.12‰ 2SD based on measurements of the internal standard University of Wisconsin Distilled Water (UWDW-2) from each day of analysis (n = 5, average = −8.94‰ raw).
[a] Samples labeled before and after are starting solutions collected before and after placing material into reaction vessels. The time difference between the two is less than 15 min.
[b] Samples marked as 5 were 5 µl samples of fluid sealed in a single glass capillary; other samples were 3 µl sealed in individual capillaries, two or three of which were loaded together for analysis.
[c] $\delta^{18}O$(VSMOW) is calculated using the average raw value of +0.15‰ for measured Standard Mean Ocean Water (SMOW) samples.
[d] $\delta^{18}O$(VSMOW-SLAP) is calculated by multiplying the VSMOW value by (−55.5/−54.76). −54.76‰ is the average for the two Standard Light Antarctic Precipitation (SLAP) samples measured; −55.5 is the accepted value.

those published for DQ from the Illinois Basin (Pollington et al., 2011; Hyodo et al., 2014) and from the Ordovician St. Peter Ss in Wisconsin (Kelly et al., 2007). Overgrowths of quartz (OQ) from outcrop set B have average $\delta^{18}O(OQ) = 30.6 \pm 2.9$‰ (2SD, n = 61, Fig. 11D) which is higher than in deeply buried rocks from the Illinois basin, but similar to $\delta^{18}O(OQ)$ values in outcrop samples of the St. Peter Ss in Wisconsin (Kelly et al., 2007).

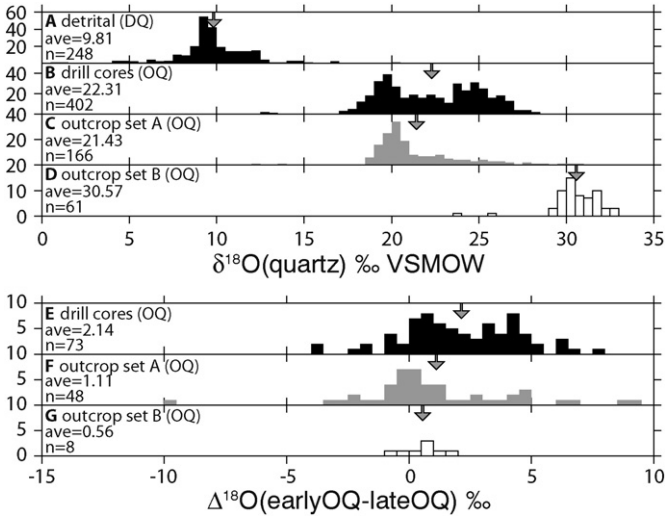

Fig. 11. Histograms of $\delta^{18}O$(Qtz) (A–D) and $\Delta^{18}O$(early OQ − late OQ) (E–G) measured by SIMS for the Mt. Simon Sandstone of Wisconsin and Illinois. Gray arrows represent the average value of each panel. (A) $\delta^{18}O$(DQ) from all samples of detrital quartz in this study as well as values from Pollington et al. (2011). (B) $\delta^{18}O$(OQ) from Illinois Basin drill core samples. (C) $\delta^{18}O$(OQ) from outcrop set A samples. (D) $\delta^{18}O$(OQ) from outcrop set B samples. (E) $\Delta^{18}O$(early-late) for OQ from Illinois Basin drill core samples. (F) $\Delta^{18}O$(early-late) for OQ from outcrop set A samples. (G) $\Delta^{18}O$(early-late) for OQ from outcrop set B samples. Note color of bars (black, gray, white) from overgrowth data corresponds between B–D and E–G. Data in panels B and E are from Pollington et al. (2011).

The detrital quartz from all samples of the Mt. Simon sandstone has $\delta^{30}Si$ values close to 0‰ (Fig. 12A, average $\delta^{30}Si(DQ) = 0.15 \pm 0.53$‰ 2SD, n = 105). These DQ values are similar to overgrowths from drill core samples (average $\delta^{30}Si(OQ) = 0.01 \pm 0.45$‰ 2SD, n = 60), all of which are consistent with a detrital source dominated by igneous quartz (Douthitt, 1982; Ding et al., 1996; Ziegler et al., 2005a; Ziegler et al., 2005b). The majority of outcrops in Wisconsin (set B) have $\delta^{30}Si(OQ)$ values indistinguishable from detrital quartz (average $\delta^{30}Si = 0.26 \pm 0.73$‰ 2SD, n = 41). Strikingly however, $\delta^{30}Si(OQ)$ from the samples from outcrop set A are considerably lower and more variable than values from any other samples in this study, ranging from −5.4 to 0.6 (n = 120). The distinct differences in diagenetic values of $\delta^{18}O$ and $\delta^{30}Si$ are clearly shown in the histograms in Figs. 11B–D and 12B–D. Both the measured values of $\delta^{30}Si(OQ)$ and $\delta^{18}O(OQ)$ from outcrop set A are highly variable and considerably lower than those measured in outcrop set B, or drill core samples (Fig. 13; $\delta^{18}O$(OQ set A) = 12.3‰ to 30.5‰, n = 166). Most of the variability observed in

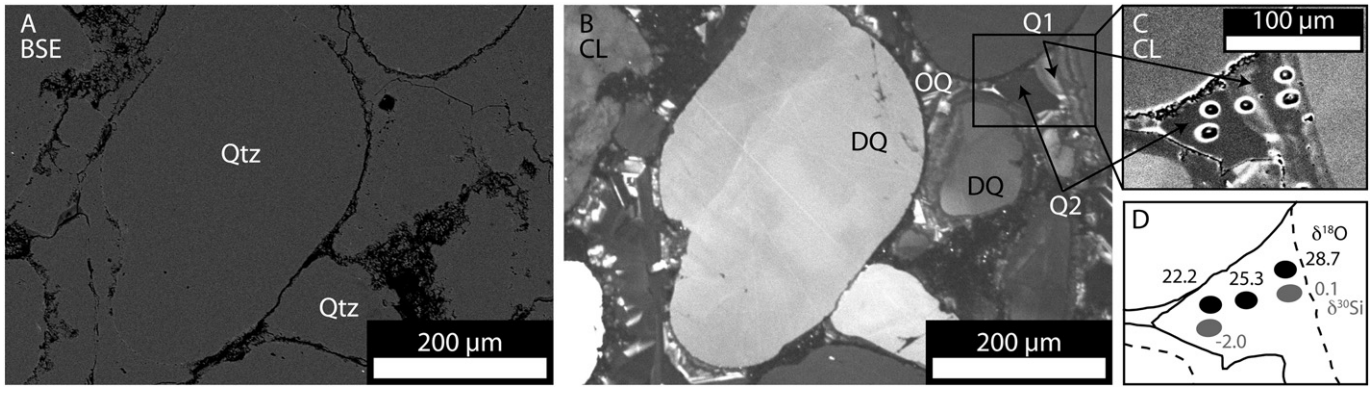

Fig. 10. Photomicrographs of Mt. Simon sample 09WI-18, outcrop set A. (A) Backscattered electron (BSE) image. All grains and overgrowths in this image are quartz (Qtz). (B) Cathodoluminescence (CL) image of the same area as panel A. Detrital quartz (DQ) and overgrowth quartz (OQ) appear the same by BSE, but are plainly distinguished by CL. (C) Inset of panel B showing SIMS analysis spots. The distinct early, bright CL texture (Q1) followed by a later dark CL domain (Q2) in the same overgrowth is clearly visible in this image. (D) Cartoon of analyses and overgrowths from panel C. The two overgrowth generations labeled with arrows have distinctly different compositions: $\delta^{18}O(Q1) = 28.7$‰ and $\delta^{30}Si(Q1) = 0.1$‰ vs. $\delta^{18}O(Q2) = 22.2$‰ and $\delta^{30}Si(Q2) = -2.0$‰.

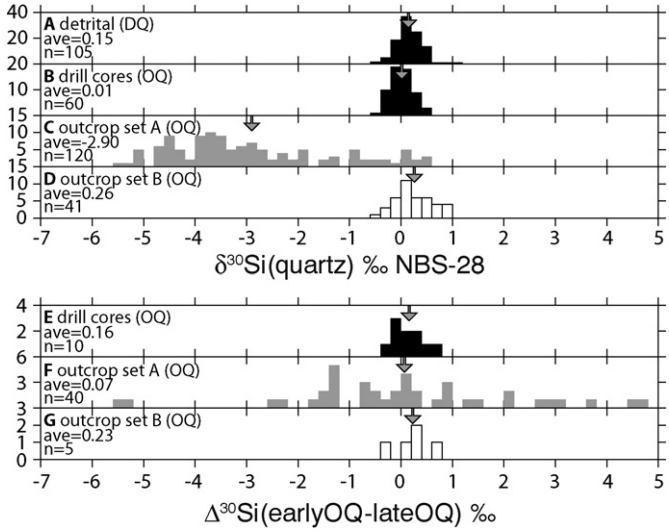

Fig. 12. Histograms of δ^{30}Si(Qtz) (A–D) and Δ^{30}Si(early OQ − late OQ) (E–G) measured by SIMS for the Mt. Simon Sandstone of Wisconsin and Illinois. Gray arrows represent the average value of each panel. (A) δ^{30}Si(DQ) from all detrital quartz samples in this study. (B) δ^{30}Si(OQ) from Illinois Basin drill core samples. (C) δ^{30}Si(OQ) from outcrop set A samples. (D) δ^{30}Si(OQ) from outcrop set B samples. (E) Δ^{30}Si(early-late) for OQ from Illinois Basin drill core samples. (F) Δ^{30}Si(early-late) for OQ from outcrop set A samples. (G) Δ^{30}Si(early-late) for OQ from outcrop set B samples. Note color of bars (black, gray, white) from overgrowth data corresponds between B–D and E–G.

δ^{18}O(OQ) and δ^{30}Si(OQ) from outcrop set A is within overgrowth generation Q2; Q1 has δ^{18}O(OQ) ~27‰ and δ^{30}Si(OQ) ~0‰, and Q3 has δ^{18}O(OQ) ~23‰ and δ^{30}Si(OQ) ~0‰ (Fig. 13). All outcrop and drill core δ^{18}O and δ^{30}Si data are included in data repository Tables ST3, ST4 and ST5.

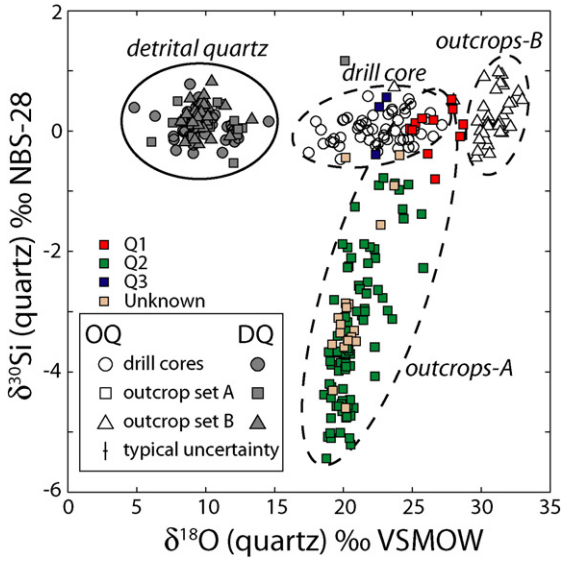

Fig. 13. Crossplot of δ^{18}O and δ^{30}Si for quartz from the Mt. Simon Sandstone measured by SIMS. Symbols are the same as Fig. 9: circles represent drill cores from the Illinois Basin, squares represent outcrop set A, triangles represent outcrop set B. Open and colored symbols represent overgrowth quartz, filled gray symbols represent detrital quartz. Outcrop set A is separated by quartz overgrowth generation (Q1, Q2, Q3, and unknown — the generation for these points is unclear, but given the similarity to other data it is likely the majority of the unknown points are Q2). The legend shows typical 2SD of 0.3‰ for both δ^{18}O and δ^{30}Si. Values of detrital grains from all datasets cluster around igneous values (δ^{18}O ≈ 10‰, δ^{30}Si ≈ 0‰) and are dominantly within the solid oval. Dashed ovals highlight individual data sets for drill core, outcrop set A, and outcrop set B. The variable δ^{18}O(OQ) values of basin samples represent growth over a range of temperatures during burial and heating (Pollington et al., 2011). The δ^{18}O(OQ) of outcrop set B samples are similar to those measured by Kelly et al. (2007) suggesting growth at a constant low temperature. Low values of δ^{30}Si and δ^{18}O of outcrop set A are interpreted to represent growth from weathered material introduced by hydrothermal fluids.

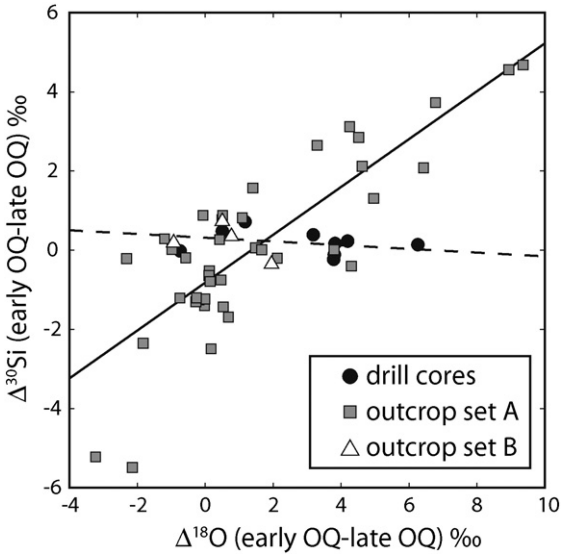

Fig. 14. Crossplot of Δ^{18}O(early OQ-late OQ) vs. Δ^{30}Si(early OQ-late OQ). Symbols are the same as Figs. 9 and 13: circles represent drill cores from the Illinois Basin, squares represent outcrop set A, triangles represent outcrop set B. Positive trend of Δ^{18}O vs. Δ^{30}Si in outcrop set A (solid line fit to measured data) is dominated by an early high δ^{18}O, high δ^{30}Si generation of cement (Q1; Fig. 10). Essentially flat trend in data from drill cores and outcrop set B (dashed line fit to measured data) reflects variability in δ^{18}O(OQ) due to temperature (IL Basin, Pollington et al., 2011) and a lack of variability in δ^{30}Si(OQ) values due to the smaller temperature coefficient of the fractionation factor derived by experiments (Fig. 8).

In quartz overgrowths large enough for two SIMS analyses (thickness 20–200 μm), the difference in δ^{30}Si between the earliest spot (i.e., closest cement to the detrital grain) and the latest spot (Δ^{30}Si(early-late)) provides an indicator of changing δ^{30}Si values over time and with progressive growth. As expected given the small total range of δ^{30}Si values, Δ^{30}Si is close to 0‰ for overgrowths from drill core samples (Fig. 12E) and samples from outcrop set B (Fig. 12G) indicating no systematic variation during progressive precipitation. Samples from outcrop set A, which have a wider range of δ^{30}Si(OQ) are also much more variable in Δ^{30}Si (Fig. 12F). High positive values of Δ^{30}Si correlate with high values of Δ^{18}O from the same overgrowths (Fig. 14). Positive values of Δ^{18}O and Δ^{30}Si are controlled by the early Q1 cement, which has δ^{30}Si ~ 0‰ and δ^{18}O ~ 28‰ compared to Q2, which has low δ^{30}Si and δ^{18}O. The highly negative Δ^{30}Si values are controlled by the difference between Q2, which has variable and low δ^{18}O and δ^{30}Si values, and Q3, which has δ^{30}Si ~ 0‰ and δ^{18}O higher than the average for these rocks.

4.7.4. Silicon isotope fractionation during chemical weathering

It has been suggested that negative values in diagenetic quartz are evidence of reprecipitation of Si fractionated during weathering (Basile-Doelsch et al., 2005). During weathering of feldspars, ^{28}Si is preferentially fractionated into the precipitated clay minerals vs. fluids leaving the solid fraction lower in δ^{30}Si and the aqueous fluid higher in δ^{30}Si (Ding et al., 1996; Ding et al., 2004; Ziegler et al., 2005a; Ziegler et al., 2005b; Georg et al., 2007). Ziegler et al. (2005a) reported results from precipitation experiments at 25–90 °C that show Si in solution is enriched in ^{30}Si by as much as ~1 to 4‰ compared to Si in precipitated minerals. In contrast, silicon isotopes are not expected to fractionate during quartz dissolution because quartz dissolves congruently.

Aqueous silicon (Si_{aq}) available to precipitate quartz overgrowths in sandstones can come from a number of sources, including: (1) congruent dissolution of quartz, either in igneous rocks or in detrital quartz grains, leading to a δ^{30}Si value ~0‰ & likely low Si_{aq} concentrations and (2) chemical weathering of non-quartz silicate minerals that causes fractionation and a δ^{30}Si value significantly different from 0‰ (either positive δ^{30}Si if it is the primary fluid derived from feldspar weathering,

or negative $\delta^{30}Si$ if the fluid contains silicon from the dissolution of previously precipitated clays). The quartz overgrowths in the majority of Mt. Simon Ss samples (all basin samples, and outcrop set B) are consistent with source (1), having $\delta^{30}Si$ values ~0‰. This suggests that these overgrowths precipitated from Si_{aq} that was largely derived by dissolution of detrital quartz that is dominantly of igneous origin and that precipitation occurred in a system that was rock-dominated with respect to Si, leading to no isotopic fractionation of Si during precipitation. The majority of diagenetic quartz in the samples from outcrop set A however appears to be dominated by Si_{aq} derived from weathering of non-quartz silicate minerals.

The results of the experimental calibration in this study, as well as calculations of Si isotope fractionation by Dupuis et al. (2015), show that under equilibrium conditions, quartz will precipitate with a higher $\delta^{30}Si$ than the corresponding fluid. In order to form the highly fractionated low-$\delta^{30}Si$(OQ) values observed in outcrop set A, it is possible that the fluids from which they precipitated were even more negative. Using a $\varepsilon^{30}Si$(Qtz–fluid) value of +1‰ (T ≈ 100 °C, based on the close agreement between experiments and calculations), assuming equilibrium fractionation the $\delta^{30}Si$(fluid) for the most negative $\delta^{30}Si$(OQ) values would have been ≈−6.5‰. However, if the Si isotope fractionation during quartz precipitation at low-temperatures in nature is dominated by kinetic rather than equilibrium processes, as suggested by the large discrepancies between the results of this study and previous empirical calibrations (Fig. 8), only moderately weathered material may be necessary to form the low $\delta^{30}Si$ (OQ) observed for the Mt. Simon Ss in outcrop set A. This scenario would still require multiple cycles of silicate weathering and precipitation to create fluids with negative $\delta^{30}Si$ values, but is consistent with values from a weathering profile in Puerto Rico ($\delta^{30}Si$(fluid) ≈ −2‰; Ziegler et al., 2005b).

The overgrowths in the Mt. Simon Ss in outcrop set B with $\delta^{30}Si$ ~ 0‰ could contain Si that is locally derived from the sandstone, or transported from another source. Regardless of the source of Si in these samples, it is clear that conditions of quartz growth and the source of Si were distinctly different in outcrop set B vs. A. The values measured for outcrop set B appear to be the more common scenario (e.g., they are comparable to values from the Illinois Basin as well as some overgrowths measured by Basile-Doelsch et al., 2005), whereas those from outcrop set A are more unusual. This may be due to the proximity of outcrop set A to a chemically distinct horizon that contained highly fractionated Si derived from chemical weathering (see discussion in Section 4.7.5).

4.7.5. Thermal and chemical history of sandstone samples

The $\delta^{18}O$(OQ) values of quartz cements from Illinois Basin samples show consistent zoning of up to 9‰ in $\delta^{18}O$ that is interpreted to reflect growth during burial and heating over a period of up to 200 million years with limited fluid flow driven by compaction and Si mainly derived by pressure solution. These results suggest little or no changes in $\delta^{18}O(H_2O)$ and that zoning of single quartz overgrowths that show systematically decreasing values of $\delta^{18}O$(OQ) are caused by increasing temperature from ~45 to 120 °C (Pollington et al., 2011; Hyodo et al., 2014). This model is consistent with a $\delta^{18}O(H_2O)$ value of −3‰, which matches estimates for Cambrian seawater (Came et al., 2007; Jaffrés et al., 2007). Even if a different value for $\delta^{18}O(H_2O)$ is used for the calculations, the up to 7.7‰ gradients in $\delta^{18}O$(OQ) seen in single overgrowths are consistent with an increase in temperature of ~70 °C during burial (Pollington et al., 2011; Hyodo et al., 2014). Using the $1000ln\alpha^{18}O(Qtz–H_2O)$ values determined in this study and $\delta^{18}O(H_2O) = -3‰$, the highest and lowest temperatures calculated for the measured $\delta^{18}O$(OQ) of Pollington et al. (2011) are 103 °C and 31 °C, compared to 107 °C and 40 °C using the calibration of Clayton et al. (1972). These differences in calculated temperature are small, demonstrating that the results of both studies represent equilibrium fractionation and that the salt effect is small for the new experiments, but the calibration from the present study is recommended because the results were defined with in situ analysis of experimental products.

The $\delta^{18}O$(OQ) values from outcrop set B are high (30.6 ± 2.9‰) and consistent with growth at near-surface temperatures, similar to what has been observed for outcrops of the St. Peter Ss in southern Wisconsin (Kelly et al., 2007). However, $\delta^{18}O$(OQ) from outcrop set A are 2 to 12‰ lower than from outcrop set B (Fig. 13), consistent with precipitation from warmer fluids. The correlated variability in $\Delta^{18}O$ and $\Delta^{30}Si$ in quartz overgrowths from outcrop set A (Fig. 14) reflects changes in the conditions of precipitation between the three generations of cement. The early cement (Q1) represents growth at cool, near-surface temperatures (similar to, although slightly different from, overgrowths from outcrop set B) whereas the majority of cement, which formed during Q2, reflects growth from warmer fluid. Finally, Q3 reflects a return to fluids consistent with Si_{aq} dominated by dissolution of detrital quartz, potentially still at warmer temperatures than those interpreted for Q1 (Fig. 13).

The sandstones at outcrop set A are less than a few meters above the Precambrian-Cambrian unconformity, which locally channeled the flow of hydrothermal fluids (Harper et al., 1995; Ziegler and Longstaffe, 2000). Where paleo-saprolites have been observed in the North American midcontinent, chemical and mineralogical indicators demonstrate weathering profiles (Driese et al., 2007; Driese and Medaris, 2008). The majority of quartz overgrowths that were analyzed for zoning have negative $\Delta^{30}Si$(earlyOQ–lateOQ) and near-zero $\Delta^{18}O$(earlyOQ–lateOQ) values (Fig. 14) that are controlled by progressive leaching of variably weathered basement rocks, or mixing with other sources of dissolved silica. These results support the following model. Before deposition of the Mt. Simon Ss, the Precambrian rocks were exposed to chemical weathering and erosion, creating horizons with residual clays low in $\delta^{30}Si$ (e.g., silcrete and clay data presented in Ziegler et al., 2005a, 2005b; Heck et al., 2011). The Precambrian saprolite at the unconformity surface experienced multiple cycles of Si-isotope fractionation creating paleosols with progressively lower $\delta^{30}Si$ clays. The paleosols were either restricted to certain environments or removed by erosion in many places, leaving localized exposures of the Precambrian basement. Later, after deposition of the Mt. Simon Ss and low temperature cementation of quartz overgrowth generation Q1 (Fig. 10), hydrothermal fluids flowing along specific zones of the unconformity (Harper et al., 1995; Ziegler and Longstaffe, 2000) dissolved low $\delta^{30}Si$ paleosols and reprecipitated Si_{aq} as quartz cements. The Si and O were thus precipitated as overgrowths in the sandstone with low $\delta^{30}Si$ derived from chemically weathered material and low $\delta^{18}O$ controlled by the relatively warm fluid (T ≈ 100 °C). The return to higher $\delta^{18}O$ and $\delta^{30}Si$ values in Q3 (Fig. 13) supports the interpretation of the warmer Q2 forming period as a relatively short-lived event, such as hydrothermal fluid flow.

5. Conclusions

Quartz precipitated under experimentally controlled chemical and thermal conditions was analyzed by SIMS for $\delta^{18}O$ and $\delta^{30}Si$ and shown to be homogenous. The $\varepsilon^{18}O(Qtz–H_2O)$ at 250 °C is 10.62 ± 0.13‰, yielding the relation $1000ln\alpha^{18}O(Qtz–H_2O) = (2.91 \pm 0.04) * 10^6/T^2$. Differences between this value and most previous estimates may be due to the incomplete exchange or the incorporation of unexchanged quartz cores in bulk measurements of previous low temperature experiments. No other study has directly measured the silicon isotope ratio of quartz and fluid from the same experiment. The $\varepsilon^{30}Si$(Qtz–fluid) value for this study is +0.55 ± 0.10‰, which is in close agreement with recent numerical predictions, but is reversed and up to 6‰ higher than previously published values that range from $\varepsilon^{30}Si(Qtz–fluid) = 0$ to −5.5‰. The experiments yield the relation $1000ln\alpha^{30}Si(Qtz–fluid) = (0.15 \pm 0.03) * 10^6/T^2$.

This study demonstrates the advantages of analyzing experimental products in situ. By targeting only quartz that grew during an experiment using an in situ SIMS technique, the uncertainties relating to mixed analyses in partially exchanged experimental products are

removed. The method described here can be applied to other systems of interest and are especially advantageous at low temperature, where experiments are hampered by slow exchange rate.

Silicon and oxygen isotopes aid in elucidating the thermal and fluid history of silica cements in the Cambrian Mt. Simon sandstone, which contains multiple generations of quartz overgrowth grown concentrically on detrital quartz grains. The detrital quartz δ^{30}Si values are close to 0‰, which is consistent with a source dominated by igneous quartz. Likewise, δ^{30}Si values are homogeneous throughout the Illinois basin and Wisconsin arch for overgrowth quartz (OQ) in the majority of the Mt. Simon Ss consistent with a source of silicon derived from pressure solution of detrital quartz. In contrast, local occurrences of very low δ^{30}Si(OQ) to −5.4‰, coupled with low δ^{18}O(OQ) from the same overgrowths document hydrothermal fluids that leached low-δ^{30}Si silicon from highly weathered Precambrian rocks. The positive ε^{30}Si(Qtz–fluid) value determined experimentally in this study indicates that precipitation of many low temperature silica cements is not an equilibrium process with respect to silicon isotopes. The extremely low δ^{30}Si(OQ) values (<−5‰) demonstrate that weathering along the Precambrian unconformity was particularly intense.

Supplementary data to this article can be found online at http://dx.doi.org/10.1016/j.chemgeo.2015.11.011.

Acknowledgments

The WiscSIMS laboratory is supervised by Noriko Kita and maintained by Jim Kern. Brian Hess prepared sample mounts and helped with preparation of quartz chips. Hiromi Konishi and Minglu Liu assisted with XRD analyses. John Fournelle and Phillip Gopon supported SEM work. Ellen Syracuse assisted in drafting figures. Samples from Illinois were provided by the Illinois State Geological Survey, with the assistance of Bob Mumm and Jared Freiburg. Wisconsin sample 07WI-1 was provided by Robert Dott, Jr. who also provided helpful discussions on earlier versions of the manuscript. Hubert King suggested methods to aid the experimental portion of the study. Preliminary analyses of similar Mt. Simon samples were performed by Andrew Trzaskus and Philipp Heck. Funding was provided by the Division of Chemical Sciences, Geosciences, and Biosciences, Office of Basic Energy Sciences, U.S. Department of Energy (93ER14389) to JWV and Graduate Student Research grants from the Geological Society of America and UW-Madison Department of Geoscience to ADP. LMA was supported by the Division of Chemical Sciences, Geosciences, and Biosciences, Office of Basic Energy Sciences, U.S. Department of Energy. The WiscSIMS laboratory is partially funded by the U.S. National Science Foundation (EAR-1053466, 1355590). Constructive reviews from Merlin Méheut, an anonymous reviewer, and Editor Michael Böttcher improved the final manuscript.

References

Abraham, K., Opfergelt, S., Fripiat, F., Cavagna, A.-J., De Jong, J.T.M., Foley, S.F., André, L., Cardinal, D., 2008. δ^{30}Si and δ^{29}Si determinations on USGS BHVO-1 and BHVO-2 reference materials with a new configuration on a Nu Plasma multi-collector ICP-MS. Geostand. Geoanal. Res. 32 (2), 193–202. http://dx.doi.org/10.1111/j.1751-908X.2008.00879.x.

Anovitz, L.M., Elam, J.M., Riciputi, L.R., Cole, D.R., 2004. Isothermal time-series determination of the rate of diffusion of water in Pachuca obsidian. Archaeometry 46, 301–326. http://dx.doi.org/10.1111/j.1475-4754.2004.00159.x.

Barkan, E., Luz, B., 2005. High precision measurements of $^{17}O/^{16}O$ and $^{18}O/^{16}O$ ratios in H_2O. Rapid Commun. Mass Spectrom. 19 (24), 3737–3742. http://dx.doi.org/10.1002/rcm.2250.

Basile-Doelsch, I., 2006. Si stable isotopes in the Earth's surface: A review. J. Geochem. Explor. 88 (1-3), 252–256. http://dx.doi.org/10.1016/j.gexplo.2005.08.050.

Basile-Doelsch, I., Meunier, J.D., Parron, C., 2005. Another continental pool in the terrestrial silicon cycle. Nature 433 (7024), 399–402. http://dx.doi.org/10.1038/nature03217.

Bottinga, Y., Javoy, M., 1973. Comments on oxygen isotope geothermometry. Earth Planet. Sci. Lett. 20 (2), 250–265.

Bowen, B.B., Ochoa, R.I., Wilkens, N.D., Brophy, J., Lovell, T.R., Fischietto, N., Medina, C.R., Rupp, J.A., 2011. Depositional and diagenetic variability within the Cambrian Mount Simon Sandstone: implications for carbon dioxide sequestration. Environ. Geosci. 18 (2), 69–89. http://dx.doi.org/10.1306/eg.07271010012.

Buschbach, T.C., 1964. Cambrian and Ordovician strata of northeastern Illinois. Illinois State Geological Survey Report of Investigations (90 pp.).

Came, R.E., Eiler, J.M., Veizer, J., Azmy, K., Brand, U., Weidman, C.R., 2007. Coupling of surface temperatures and atmospheric CO_2 concentrations during the Palaeozoic Era. Nature 449, 198–201. http://dx.doi.org/10.1038/nature06085.

Chacko, T., Cole, D.R., Horita, J., 2001. Equilibrium oxygen, hydrogen and carbon isotope fractionation factors applicable to geologic systems. In: Valley, J.W., Cole, D.R. (Eds.), Stable Isotope GeochemistryReviews in Mineralogy and Geochemistry 43. Mineralogical Society of America, pp. 1–81.

Chen, Z.S., Riciputi, L.R., Mora, C.I., Fishman, N.S., 2001. Regional fluid migration in the Illinois Basin: evidence from *in situ* oxygen isotope analysis of authigenic K-feldspar and quartz from the Mount Simon Sandstone. Geology 29 (12), 1067–1070. http://dx.doi.org/10.1130/0091-7613(2001)029<1067:RFMITI>2.0.CO;2.

Clayton, R.N., Mayeda, T.K., O'Neil, J.R., 1972. Oxygen isotope exchange between quartz and water. J. Geophys. Res. 77 (17), 3057–3067. http://dx.doi.org/10.1029/JB077i017p03057.

Clayton, R.N., Goldsmith, J.R., Mayeda, T.K., 1989. Oxygen isotope fractionation in quartz, albite, anorthite and calcite. Geochim. Cosmochim. Acta 53 (3), 725–733. http://dx.doi.org/10.1016/0016-7037(89)90015-X.

Craig, H., 1957. Isotopic standards for carbon and oxygen and correction factors for mass-spectrometric analysis of carbon dioxide. Geochim. Cosmochim. Acta 12 (1-2), 133–149. http://dx.doi.org/10.1016/0016-7037(57)90024-8.

De La Rocha, C.L., 2003. Silicon isotope fractionation by marine sponges and the reconstruction of the silicon isotope composition of ancient deep water. Geology 31 (5), 423–426. http://dx.doi.org/10.1130/0091-7613(2003)031<0423:SIFBMS>2.0.CO;2.

De La Rocha, C.L., Brzezinski, M.A., DeNiro, M.J., 1997. Fractionation of silicon isotopes by marine diatoms during biogenic silica formation. Geochim. Cosmochim. Acta 61 (23), 5051–5056. http://dx.doi.org/10.1016/S0016-7037(97)00300-1.

Delstanche, S., Opfergelt, S., Cardinal, D., Elsass, F., André, L., Delvaux, B., 2009. Silicon isotopic fractionation during adsorption of aqueous monosilicic acid onto iron oxide. Geochim. Cosmochim. Acta 73 (4), 923–934. http://dx.doi.org/10.1016/j.gca.2008.11.014.

Ding, T., Jiang, S., Wan, D., Li, Y., Li, J., Song, H., Liu, Z., Yao, X., 1996. Silicon Isotope Geochemistry. Geological Publishing House. Beijing (125 pp.).

Ding, T., Wan, D., Wang, C., Zhang, F., 2004. Silicon isotope compositions of dissolved silicon and suspended matter in the Yangtze River, China. Geochim. Cosmochim. Acta 68 (2), 205–216. http://dx.doi.org/10.1016/S0016-7037(03)00264-3.

Douthitt, C.B., 1982. The geochemistry of the stable isotopes of silicon. Geochim. Cosmochim. Acta 46 (8), 1449–1458. http://dx.doi.org/10.1016/0016-7037(82)90278-2.

Dove, P.M., 1994. The dissolution kinetics of quartz in sodium chloride solutions at 25 °C to 300 °C. Am. J. Sci. 294 (6), 665–712. http://dx.doi.org/10.2475/ajs.294.6.665.

Driese, S.G., 1979. Paleoenvironments of the Upper Cambrian Mt. Simon formation in western and west-central Wisconsin (M. S. Thesis) University of Wisconsin-Madison (207 pp.).

Driese, S.G., Medaris, L.G., 2008. Evidence for biological and hydrological controls on the development of a Paleoproterozoic paleoweathering profile in the Baraboo Range, Wisconsin, USA. J. Sediment. Res. 78 (7-8), 443–457. http://dx.doi.org/10.2110/jsr.2008.051.

Driese, S.G., Medaris, L.G., Ren, M.H., Runkel, A.C., Langford, R.P., 2007. Differentiating pedogenesis from diagenesis in early terrestrial paleoweathering surfaces formed on granitic composition parent materials. J. Geol. 115 (4), 387–406. http://dx.doi.org/10.1086/518048.

Dupuis, R., Benoit, M., Nardin, E., Méheut, M., 2015. Fractionation of silicon isotopes in liquids: The importance of configurational disorder. Chem. Geol. 396, 239–254. http://dx.doi.org/10.1016/j.chemgeo.2014.12.027.

Epstein, S., Mayeda, T., 1953. Variation of ^{18}O content of waters from natural sources. Geochim. Cosmochim. Acta 4 (5), 213–224. http://dx.doi.org/10.1016/0016-7037(53)90051-9.

Friedman, I., O'Neil, J.R., 1977. Compilation of stable isotope fractionation factors of geochemical interest. United States Geological Survey professional paper 440-KK, Washington, D.C. (67 pp.)

Geilert, S., Vroon, P.Z., Roerdink, D.L., Van Cappellen, P., van Bergen, M.J., 2014. Silicon isotope fractionation during abiotic silica precipitation at low temperatures: inferences from flow-through experiments. Geochim. Cosmochim. Acta 142, 95–114. http://dx.doi.org/10.1016/j.gca.2014.07.003.

Georg, R.B., Reynolds, B.C., Frank, M., Halliday, A.N., 2006. New sample preparation techniques for the determination of Si isotopic compositions using MC-ICPMS. Chem. Geol. 235 (1-2), 95–104. http://dx.doi.org/10.1016/j.chemgeo.2006.06.006.

Georg, R.B., Reynolds, B.C., West, A.J., Burton, K.W., Halliday, A.N., 2007. Silicon isotope variations accompanying basalt weathering in Iceland. Earth Planet. Sci. Lett. 261 (3-4), 476–490. http://dx.doi.org/10.1016/j.epsl.2007.07.004.

Georg, R.B., Zhu, C., Reynolds, B.C., Halliday, A.N., 2009. Stable silicon isotopes of groundwater, feldspars, and clay coatings in the Navajo Sandstone aquifer, Black Mesa, Arizona, USA. Geochim. Cosmochim. Acta 73 (8), 2229–2241. http://dx.doi.org/10.1016/j.gca.2009.02.005.

Harper, D.A., Longstaffe, F.J., Wadleigh, M.A., Mcnutt, R.H., 1995. Secondary K-Feldspar at the Precambrian–Paleozoic unconformity, Southwestern Ontario. Can. J. Earth Sci. 32 (9), 1432–1450. http://dx.doi.org/10.1139/e95-116.

Heck, P.R., Huberty, J.M., Kita, N.T., Ushikubo, T., Kozdon, R., Valley, J.W., 2011. SIMS analyses of silicon and oxygen isotope ratios for quartz from Archean and Paleoproterozoic banded iron formations. Geochim. Cosmochim. Acta 75, 5879–5891. http://dx.doi.org/10.1016/j.gca.2011.07.023.

Hoholick, J.D., Metarko, T., Potter, P.E., 1984. Regional variations of porosity and cement: St. Peter and Mount Simon Sandstones in Illinois Basin. AAPG Bull. 68 (6), 753–764.

Horita, J., Cole, D.R., Wesolowski, D.J., 1993a. The activity-composition relationship of oxygen and hydrogen isotopes in aqueous salt solutions: II. Vapor–liquid water equilibration of mixed salt solutions from 50 to 100 °C and geochemical implications.

Geochim. Cosmochim. Acta 57 (19), 4703–4711. http://dx.doi.org/10.1016/0016-7037(93)90194-2.
Horita, J., Wesolowski, D.J., Cole, D.R., 1993b. The activity-composition relationship of oxygen and hydrogen isotopes in aqueous salt solutions: I. Vapor–liquid water equilibration of single salt solutions from 50 to 100 °C. Geochim. Cosmochim. Acta 57 (12), 2797–2817. http://dx.doi.org/10.1016/0016-7037(93)90391-9.
Horita, J., Cole, D.R., Wesolowski, D.J., 1995. The activity–composition relationship of oxygen and hydrogen isotopes in aqueous salt solutions: III. Vapor–liquid water equilibration of NaCl solutions to 350 °C. Geochim. Cosmochim. Acta 59 (6), 1139–1151. http://dx.doi.org/10.1016/0016-7037(95)00031-T.
Hu, G.X., Clayton, R.N., 2003. Oxygen isotope salt effects at high pressure and high temperature and the calibration of oxygen isotope geothermometers. Geochim. Cosmochim. Acta 67 (17), 3227–3246. http://dx.doi.org/10.1016/S0016-7037(02)01319-4.
Hyodo, A., Kozdon, R., Pollington, A.D., Valley, J.W., 2014. Evolution of quartz cementation and burial history of the Eau Claire Formation based on *in situ* oxygen isotope analysis of quartz overgrowths. Chem. Geol. 384, 168–180. http://dx.doi.org/10.1016/j.chemgeo.2014.06.021.
Jabeen, I., Kusakabe, M., 1997. Determination of $\delta^{17}O$ values of reference water samples VSMOW and SLAP. Chem. Geol. 143 (1-2), 115–119. http://dx.doi.org/10.1016/S0009-2541(97)00109-5.
Jaffrés, J.B.D., Shields, G.A., Wallmann, K., 2007. The oxygen isotope evolution of seawater: a critical review of a long-standing controversy and an improved geological water cycle model for the past 3.4 billion years. Earth Sci. Rev. 83, 83–122. http://dx.doi.org/10.1016/j.earscirev.2007.04.002.
Kawabe, I., 1978. Calculation of oxygen isotope fractionation in quartz–water system with special reference to low-temperature fractionation. Geochim. Cosmochim. Acta 42 (6), 613–621. http://dx.doi.org/10.1016/0016-7037(78)90006-6.
Kelly, J.L., Fu, B., Kita, N.T., Valley, J.W., 2007. Optically continuous silcrete quartz cements of the St. Peter Sandstone: high precision oxygen isotope analysis by ion microprobe. Geochim. Cosmochim. Acta 71 (15), 3812–3832. http://dx.doi.org/10.1016/j.gca.2007.05.014.
Kita, N.T., Ushikubo, T., Fu, B., Valley, J.W., 2009. High precision SIMS oxygen isotope analysis and the effect of sample topography. Chem. Geol. 264 (1-4), 43–57. http://dx.doi.org/10.1016/j.chemgeo.2009.02.012.
Kusakabe, M., Matsuhisa, Y., 2008. Oxygen three-isotope ratios of silicate reference materials determined by direct comparison with VSMOW-oxygen. Geochem. J. 42 (4), 309–317. http://dx.doi.org/10.2343/geochemj.42.309.
Lander, R.H., Larese, R.E., Bonnell, L.M., 2008. Toward more accurate quartz cement models: The importance of euhedral versus noneuhedral growth rates. AAPG Bull. 92 (11), 1537–1563. http://dx.doi.org/10.1306/07160808037.
Leetaru, H.E., Freiburg, J.T., 2014. Litho-facies and reservoir characterization of the Mt. Simon Sandstone at the Illinois Basin — Decatur Project. Greenhouse Gases Sci. Technol. 4 (5), 580–595. http://dx.doi.org/10.1002/ghg.1453.
Li, Y., Ding, T., Wan, D., 1995. Experimental study of silicon isotope dynamic fractionation and its application in geology. Chin. J. Geochem. 14, 212–219. http://dx.doi.org/10.1007/BF02842044.
Mackenzie, F.T., Gees, R., 1971. Quartz: Synthesis at earth-surface conditions. Science 173 (3996), 533–535. http://dx.doi.org/10.1126/science.173.3996.533.
Mai, H., Dott Jr., R.H., 1985. A subsurface study of the St. Peter Sandstone in southern and eastern Wisconsin. Wisconsin Geological and Natural History Survey Information Circular 47. 47 (26 pp.).
Matsuhisa, Y., Goldsmith, J.R., Clayton, R.N., 1978. Mechanisms of hydrothermal crystallization of quartz at 250 °C and 15 Kbar. Geochim. Cosmochim. Acta 42 (2), 173–182. http://dx.doi.org/10.1016/0016-7037(78)90130-8.
Matsuhisa, Y., Goldsmith, J.R., Clayton, R.N., 1979. Oxygen isotopic fractionation in the system quartz–albite–anorthite–water. Geochim. Cosmochim. Acta 43 (7), 1131–1140. http://dx.doi.org/10.1016/0016-7037(79)90099-1.
Méheut, M., Schauble, E.A., 2014. Silicon isotope fractionation in silicate minerals: insights from first-principles models of phyllosilicates, albite and pyrope. Geochim. Cosmochim. Acta 134, 137–154. http://dx.doi.org/10.1016/j.gca.2014.02.014.
Oelze, M., von Blanckenburg, F., Hoellen, D., Dietzel, M., Bouchez, J., 2014. Si stable isotope fractionation during adsorption and the competition between kinetic and equilibrium isotope fractionation: implications for weathering systems. Chem. Geol. 380, 161–171. http://dx.doi.org/10.1016/j.chemgeo.2014.04.027.
O'Neil, J.R., Epstein, S., 1966. A method for oxygen isotope analysis of milligram quantities of water and some of its applications. J. Geophys. Res. 71 (20), 4955–4961. http://dx.doi.org/10.1029/JZ071i020p04955.
Peres, P., Kita, N.T., Valley, J.W., Fernandes, F., Schuhmacher, M., 2013. New sample holder geometry for high precision isotope analyses. Surf. Interface Anal. 45 (1), 553–556. http://dx.doi.org/10.1002/sia.5061.
Pollington, A.D., Kozdon, R., Valley, J.W., 2011. Evolution of quartz cementation during burial of the Cambrian Mount Simon Sandstone, Illinois Basin: *in situ* microanalysis of $\delta^{18}O$. Geology 39 (12), 1119–1122. http://dx.doi.org/10.1130/G32195.1.
Reddy, T.R., Zheng, X.-Y., Beard, B.L., Johnson, C.M., 2015. Si isotope fractionation during reductive dissolution of Fe-Si gel in Artifical Archean Sewater (AAS) by *Desulfuromonas acetoxidans*. Astrobiology Science Conference (AbSciCon 2015), Chicago, IL.
Roerdink, D.L., van den Boorn, S.H.J.M., Geilert, S., Vroon, P.Z., van Bergen, M.J., 2015. Experimental constraints on kinetic and equilibrium silicon isotope fractionation during the formation of non-biogenic chert deposits. Chem. Geol. 402, 40–51. http://dx.doi.org/10.1016/j.chemgeo.2015.02.038.
Sharp, Z.D., Kirschner, D.L., 1994. Quartz-calcite oxygen isotope thermometry: a calibration based on natural isotopic variations. Geochim. Cosmochim. Acta 58 (20), 4491–4501. http://dx.doi.org/10.1016/0016-7037(94)90350-6.
Shiro, Y., Sakai, H., 1972. Calculation of reduced partition-function ratios of α-, β-quartzs and calcite. Bull. Chem. Soc. Jpn. 45 (8), 2355–2359. http://dx.doi.org/10.1246/bcsj.45.2355.
Spicuzza, M.J., Valley, J.W., Kohn, M.J., Girard, J.P., Fouillac, A.M., 1998a. The rapid heating, defocused beam technique: a CO_2-laser-based method for highly precise and accurate determination of $\delta^{18}O$ values of quartz. Chem. Geol. 144 (3-4), 195–203. http://dx.doi.org/10.1016/S0009-2541(97)00131-9.
Spicuzza, M.J., Valley, J.W., McConnell, V.S., 1998b. Oxygen isotope analysis of whole rock via laser fluorination; an air-lock approach. Abstracts with Programs - Geological Society of America 30(7), p. 80.
Stumm, W., Morgan, J.J., 1996. Aquatic Chemistry: Chemical equilibria and rates in natural waters. Wiley, New York (1024 pp.).
Templeton Jr., J.S., 1951. The Mt. Simon Sandstone in Northern Illinois. Illinois Geological Survey Circular. 170, pp. 151–159.
Urey, H.C., 1947. The thermodynamic properties of isotopic substances. J. Chem. Soc. (Resumed) 562–581 http://dx.doi.org/10.1039/JR9470000562.
Valley, J.W., Kita, N.T., 2009. *In situ* oxygen isotope geochemistry by ion microprobe. In: Fayek, M. (Ed.), Secondary Ion Mass Spectrometry in the Earth Sciences: Gleaning the big picture from a small spotShort Course Series 41. Mineralogical Association of Canada, pp. 19–63.
Valley, J.W., Kitchen, N., Kohn, M.J., Niendorf, C.R., Spicuzza, M.J., 1995. UWG-2, a garnet standard for oxygen isotope ratios: strategies for high precision and accuracy with laser heating. Geochim. Cosmochim. Acta 59 (24), 5223–5231. http://dx.doi.org/10.1016/0016-7037(95)00386-X.
Walderhaug, O., 1994. Precipitation rates for quartz cement in sandstones determined by fluid-inclusion microthermometry and temperature-history modeling. J. Sediment. Res. A-Sediment. Petrol. Process. 64 (2), 324–333. http://dx.doi.org/10.2110/jsr.64.324.
Wang, X.-L., Coble, M.A., Valley, J.W., Shu, X.-J., Kitajima, K., Spicuzza, M.J., Sun, T., 2014. Influence of radiation damage on Late Jurassic zircon from southern China: evidence from in situ measurements of oxygen isotopes, laser Raman, U-Pb ages, and trace elements. Chem. Geol. 389, 122–136. http://dx.doi.org/10.1016/j.chemgeo.2014.09.013.
Wesolowski, D.J., Ziemniak, S.E., Anovitz, L.M., Machesky, M.L., Bénézeth, P., Palmer, D.A., 2004. Solubility and surface adsorption characteristics of metal oxides. In: Palmer, D.A., Fernández-Prini, R., Harvey, A.H. (Eds.), Aqueous Systems at Elevated Temperatures and Pressures: Physical Chemistry in Water. Elsevier, Steam and Hydrothermal Solutions, pp. 492–595 http://dx.doi.org/10.2172/821956.
Willman, H.B., Atherton, E., Buschbach, T.C., Collinson, C., Frye, J.C., Hopkins, M.E., Lineback, J.A., Simon, J.A., 1975. Handbook of Illinois stratigraphy. Illinois State Geological Survey Bulletin (261 pp.).
Worden, R.H., Morad, S., 2000. Quartz cementation in oil field sandstones: a review of the key controversies. In: Worden, R., Morad, S. (Eds.), Quartz cementation in sandstones. International Association of Sedimentologists Special publication 29. Blackwell Science, Malden, MA, pp. 1–20. http://dx.doi.org/10.1002/9781444304237.ch1.
Zambardi, T., Poitrasson, F., 2011. Precise determination of silicon isotopes in silicate rock reference materials by MC-ICP-MS. Geostand. Geoanal. Res. 35 (1), 89–99. http://dx.doi.org/10.1111/j.1751-908X.2010.00067.x.
Zheng, Y.F., 1993. Calculation of oxygen isotope fractionation in anhydrous silicate minerals. Geochim. Cosmochim. Acta 57 (5), 1079–1091. http://dx.doi.org/10.1016/0016-7037(93)90042-U.
Zheng, X.-Y., Beard, B.L., Reddy, T.R., Johnson, C.M., 2015. Exploring silicon isotope fractionation between Precambrian-like artifical seawater and Fe–Si gel. Astrobiology Science Conference (AbSciCon 2015), Chicago, IL.
Ziegler, K., Longstaffe, F.J., 2000. Clay mineral authigenesis along a mid-continental scale fluid conduit in Palaeozoic sedimentary rocks from southern Ontario, Canada. Clay Miner. 35 (1), 239–260. http://dx.doi.org/10.1180/000985500546620.
Ziegler, K., Chadwick, O.A., Brzezinski, M.A., Kelly, E.F., 2005a. Natural variations of $\delta^{30}Si$ ratios during progressive basalt weathering, Hawaiian Islands. Geochim. Cosmochim. Acta 69 (19), 4597–4610. http://dx.doi.org/10.1016/j.gca.2005.05.008.
Ziegler, K., Chadwick, O.A., White, A.F., Brzezinski, M.A., 2005b. $\delta^{30}Si$ systematics in a granitic saprolite, Puerto Rico. Geology 33 (10), 817–820. http://dx.doi.org/10.1130/G21707.1.